Draft version February 2, 2008
Preprint typeset using LaTeX style emulateapj v. 04/03/99

M31 GLOBULAR CLUSTER X-RAY SOURCES: *XMM-NEWTON* AND *CHANDRA* RESULTS.

Sergey Trudolyubov[1,2,3] and William Priedhorsky[2]

Draft version February 2, 2008

ABSTRACT

We present the results of M31 globular cluster (GC) X-ray source survey, based on the data of *XMM-Newton* and *Chandra* observations covering ~ 6100 arcmin^2 of M31. We detected 43 X-ray sources coincident with globular cluster candidates from various optical surveys.

The inferred isotropic X-ray luminosities of GC sources lie between $\sim 10^{35}$ and $\sim 10^{39}$ erg s^{-1} in the $0.3-10$ keV energy band. The spectral properties of 31 brightest sources from our sample were found to be similar to that of the low mass X-ray binaries located in the bulge and globular clusters of the Milky Way Galaxy. The spectral distribution of M31 GC X-ray sources is consistent with that derived for the bulge of M31 and other nearby galaxies of different morphological type. Several sources demonstrate a correlation between the level of X-ray flux and hardness of their energy spectrum reminiscent of the Galactic Z and atoll sources.

We found that $\sim 80\%$ of the M31 GC sources with multiple flux measurements available show significant variability on a time scales from days to years. The X-ray source RX J0043.2+4127, coincident with GC Bo 163, has been found to show recurrent transient outbursts with peak luminosities of $\sim 10^{38}$ ergs s^{-1}. Several sources in our sample show significant variability on a time scale of individual observations, ranging from aperiodic fluctuations to regular dipping.

The X-ray luminosity function of GC sources is found to be significantly different from that of the point sources in the bulge and disk of M31. The luminosity distribution of M31 GC sources has ~ 10 times higher peak luminosity and much higher fraction of bright sources than the Milky Way GC distribution. Six persistent sources in our sample (or $\sim 14\%$ of the total number) have luminosities exceeding 10^{38} ergs s^{-1} during all observations, and three other sources occasionally exceed that luminosity level. Our observations indicate that GC sources make dominant contribution to the bright source counts in the areas of M31 covered by the survey: $\sim 40\%$ of the total number of sources with luminosities above 10^{37} ergs s^{-1} reside in GCs with fraction of GC sources rising to $67-90\%$ for the luminosities above 10^{38} ergs s^{-1}. The contribution of the GC sources to the total number of bright sources found in M31 is much higher than in the Milky Way galaxy, but surprisingly close to the early-type galaxies. We found that brightest M31 GC sources tend to reside at large galactocentric distances outside the central bulge.

We found that globular clusters hosting bright X-ray sources are optically brighter and more metal rich than the rest of M31 globular clusters, in agreement with previous studies. The brightest sources with luminosities above $\sim 10^{38}$ ergs s^{-1} show tendency to reside in more metal poor clusters.

The remarkable similarities between the properties of the M31 GC X-ray sources and that of the Galactic neutron star LMXBs allow us expect most of the persistent M31 GC X-ray sources to be LMXB systems with neutron star primaries. However, the current X-ray spectral and timing data can not rule out the possibility of finding an active accreting black holes in our GC source sample.

1. INTRODUCTION

Globular clusters (GCs) provide us with crucial information on galaxy structure and formation mechanisms. They are also ideal laboratories for studying stellar populations and evolution of dense stellar systems. X-ray surveys revealed a number of bright X-ray sources associated with Milky Way (MW) GCs and identified with low-mass X-ray binaries (LMXBs) (Hertz & Grindlay 1983, Verbunt et al. 1995). The ratio of LMXBs to stellar mass is two orders of magnitude higher for GCs than for the rest of our Galaxy (Liu et al. 2001). This overabundance of LMXB has been explained by dynamical effects such as tidal capture and three/four body interactions in the high stellar density environment (Clark 1975, Fabian, Pringle & Rees 1975). The number of known Galactic GCs hosting bright X-ray sources ($L_X > 10^{36}$ ergs s^{-1}) is pretty small: there are fourteen such systems (Liu et al. 2001). The presence of Type I X-ray bursts indicates that all luminous GC sources contain accreting neutron stars rather than black holes. With the advent of the modern X-ray observatories, it has become possible to study the X-ray properties of GCs associated with the nearby galaxies (Angelini, Loewenstein & Mushotzky 2001; Di Stefano et al. 2002; Kundu, Maccarone, & Zepf 2002). Based on a large number of objects, the extragalactic GC X-ray sources allow a broad range of statistical population studies, impossible with a limited sample of Galactic GC X-ray sources.

The Andromeda Galaxy (M31), the closest giant spiral galaxy to our own, is a unique object for the study of optical and X-ray astronomy. Its proximity and favorable

[1]IGPP, University of California, Riverside, CA 92521
[2]Los Alamos National Laboratory, Los Alamos, NM 87545
[3]Space Research Institute, Russian Academy of Sciences, Profsoyuznaya 84/32, Moscow, 117810 Russia

orientation allow to observe stellar populations over the full extent of the galaxy at a nearly uniform distance, and with less severe effects of line-of-sight contamination from interstellar gas and dust. Due to similarities between the two galaxies, the results from the study of M31 provide an important benchmark for comparison with the results from the study of our own Milky Way Galaxy. The Andromeda Galaxy possesses a significantly more populous globular cluster system than the Milky Way with more than 430 confirmed candidate members (Barmby et al. 2000). Optical studies of the Milky Way and M31 globular cluster systems have revealed that these two populations exhibit some remarkable similarities (van den Bergh 2000).

M31 was observed extensively with *Einstein*, *ROSAT*, *Chandra* and *XMM* missions, detected hundreds of sources, with bright GC X-ray sources among them (Trinchieri & Fabbiano 1991; Primini et al. 1993; Supper et al. 1997; Shirey et al. 2001). Twenty-one X-ray sources discovered with *Einstein* were tentatively identified with GCs. Based on these early results, it has been noted that the luminosities of the M31 GC sources are higher than any observed for Galactic GCs (Long & van Speybroek 1983), and that the fraction of M31 GCs with X-ray sources might be larger than the fraction in the Milky Way (Battistini et al. 1987). Observations of the central bulge of M31 with *ROSAT*/HRI detected 18 GC X-ray sources and placed upper limits on the X-ray flux from 32 other globular clusters (Primini et al. 1993). Primini, Forman & Jones (1993) found that the luminosity distribution of M31 GC sources contains a larger population of high luminosity sources than that of the Milky Way GC X-ray sources, although the peak luminosities of the two distributions were roughly comparable. The *ROSAT*/PSPC survey covering most of M31 revealed 31 X-ray sources coincident with M31 GC candidates (Supper et al. 1997, 2001). Based on this larger sample, Supper et al. (1997, 2001) concluded that there is no significant difference between the luminosity distributions of the M31 GC X-ray sources and their Galactic counterparts. Recent *Chandra* observations covering central bulge of and two regions in the northern and southern disk revealed 28 GC X-ray sources with 15 of them newly discovered (Di Stefano et al. 2002). Approximately $\sim 30\%$ of all GC sources detected in *Chandra* observations have $0.5-7$ keV luminosities above 10^{37} ergs s^{-1} and $\sim 10\%$ of all the sources have luminosities of 10^{38} ergs s^{-1} and higher. Both the peak X-ray luminosity and relative fraction of the bright sources with $L_X > 10^{37}$ ergs s^{-1} were found to be significantly higher for the *Chandra* GC source sample than for the GC sources in our Galaxy (Di Stefano et al. 2002) in contrast to the earlier *ROSAT* results (Supper et al. 1997, 2001). The limited sensitivity of *Chandra* observations allowed to study spectral properties and variability of only five most luminous sources found to be consistent with properties of the Galactic sources.

We present the results of M31 globular cluster (GC) X-ray source survey, based on the data of *XMM-Newton* and *Chandra* observations covering ~ 6100 arcmin^2 of the Andromeda galaxy (M31). The unique combination of the unprecedented sensitivity of *XMM-Newton* and superior spatial resolution of *Chandra* observations allows accurate localization and detailed study of spectral and timing properties of the GC X-ray sources in both central regions of M31 and at large galactocentric distances. We concentrate on the analysis of spectral properties and variability of individual bright sources and study a group properties of all GC X-ray sources detected in our survey. We study the relation between the properties of the X-ray sources and that of the globular clusters hosting them. Finally, the properties of M31 GC X-ray sources are compared to the properties of low-mass X-ray binaries LMXB in M31, Milky Way and other galaxies of different morphological types.

2. OBSERVATIONS AND DATA ANALYSIS

In the following analysis we used the data of 10 *XMM-Newton* observations of various M31 fields (Table 1; Fig. 1). All *XMM-Newton* observations described in this paper were performed as a part of the Performance Verification and Guaranteed Time Programs (Shirey et al. 2001, Trudolyubov et al. 2002a, Trudolyubov et al. 2002b). Four *XMM* observations cover the central bulge of M31, five – its northern and southern disk regions, and one – a distant M31 globular cluster G1 (Mayall II) field. In the following analysis we use the data of three European Photon Imaging Camera (EPIC) instruments: two EPIC MOS detectors (Turner et al. 2001) and EPIC-pn detector (Strueder et al. 2001). During all observations EPIC instruments were operated in the *full window* mode ($30'$ FOV) with *medium* or *thin* optical blocking filter.

We reduced EPIC data with the *XMM-Newton* Science Analysis System (SAS v 5.3) [4]. We performed standard screening of the EPIC data to exclude time intervals with high background levels. Images in the celestial coordinates with a pixel size of $2''$ have been accumulated in the $0.3-7.0$ keV energy band for the EPIC-MOS1, MOS2 and pn detectors. To generate lightcurves and spectra of X-ray sources, we used elliptical extraction regions with semi-axes size of $\sim 20-80''$ (depending on the distance of the source from the telescope axis) and subtracted as background the spectrum of adjacent source-free regions with subsequent normalization by a ratio of the detector areas. We corrected the count rates of the sources for the vignetting of the XMM telescope, based on the Current Calibration Files.We used data in the $0.3-10$ keV energy band because of the uncertainties in the calibration of the EPIC instruments outside this range. All fluxes and luminosities derived from spectral analysis apply to this band, unless specified otherwise. We used spectral response matrices generated by XMM SAS tasks. The EPIC count rates were converted into energy fluxes in the $0.3-10$ keV energy band using analytical fits to the spectra for brighter sources or PIMMS[5], assuming standard parameters: an absorbed simple power law model with $N_{\rm H} = 7 \times 10^{20}$ cm^{-2} and photon index $\alpha = 1.7$ (Shirey et al. 2001).

We analyzed a series of publicly available *Chandra* data for M31 fields containing optically identified GC candidates consisting of 36 observations with the Advanced CCD Imaging Spectrometer (ACIS) and 3 High Resolution Camera (HRC) observations (Table 2; Fig. 1). A more detailed description of these observations can be found in

[4]See http://xmm.vilspa.esa.es/user

[5]See http://heasarc.gsfc.nasa.gov/Tools/w3pimms.html

Garcia et al. (2000), DiStefano et al. (2002), Kong et al. (2002) and Kaaret et al. (2002).

The data of *Chandra* observations was processed using the CIAO v3.0[6] threads. We performed standard screening of the *Chandra* data to exclude time intervals with high background levels. Images in the celestial coordinates with a pixel size of $1''$ have been accumulated in the $0.3-7.0$ keV energy band for source detection procedure. Only data in the $0.3-7.0$ and $0.5-7.0$ keV energy ranges was used in the spectral analysis of ACIS-S and ACIS-I observations. To estimate energy fluxes and spectra, we extracted counts within source elliptical region with semi-axes of $3''-40''$ (depending on the source distance from the telescope axis). Background counts were extracted from the adjacent source-free regions with subsequent normalization by ratio of detector areas. To account for the continuous degradation in the effective low-energy quantum efficiency of the ACIS detectors[7], we performed correction of the spectral response files applying *ACISABS* model to the ARF files. For a few brightest GC sources pileup fraction in their ACIS spectra is estimated to be at the level of $\sim 10-30\%$. In some cases, to correct for a pileup effect in the ACIS spectra, we extracted source spectrum from the PSF wings, where the source count rate is low enough that pileup effect can be ignored. We also used Sherpa[8] implementation of the pileup model by Davis (2001,2003). The ACIS count rates were converted into energy fluxes in the $0.3-10$ keV energy band using analytical fits to the spectra for brighter sources or using PIMMS with spectral parameters derived from more sensitive observations or standard parameters otherwise. For the HRC count rates the source fluxes were estimated with PIMMS, based on the observed count rates and spectral parameters measured with *XMM*/EPIC and *Chandra*/ACIS.

For both *XMM-Newton* and *Chandra* data, X-ray sources were detected with the program based on the wavelet decomposition algorithm, set at a 4σ threshold. For our current analysis of *XMM-Newton* observations, we expect error in the source position determination to be dominated by residual systematic error of the order $1-3''$.

We performed a spectral and timing study of the brightest X-ray sources with total number of counts larger than 300. Spectra were grouped to contain a minimum of 20 counts per spectral bin and fit to analytical models using the XSPEC v.11[9] fitting package (Arnaud 1996). EPIC-pn, MOS1 and MOS2 data were fitted simultaneously, but with independent normalizations.

We studied timing properties of all bright X-ray sources detected in our observations. Fourier power density spectra (PDS) were produced using the lightcurves in the $0.3-7.0$ keV energy band. Then we performed folding analysis in the vicinity of the frequency peaks identified from PDS. We used standard XANADU/XRONOS v.5 [10] tasks to perform analysis of the timing properties of bright X-ray sources.

In the following analysis we assume a source distance of 760 kpc (van den Bergh 2000).

[6]http://asc.harvard.edu/ciao/

[7]http://cxc.harvard.edu/cal/Acis/Cal prods/qeDeg/

[8]http://cxc.harvard.edu/sherpa/

[9]http://heasarc.gsfc.nasa.gov/docs/xanadu/xspec/index.html

[10]http://heasarc.gsfc.nasa.gov/docs/xanadu/xronos/xronos.html

3. M31 GC X-RAY SOURCES: IDENTIFICATION.

The positions of 43 X-ray sources detected in the *XMM-Newton* and *Chandra* observations of M31 are consistent with globular cluster candidates from optical surveys. We used the following catalogs for identifying GC X-ray source candidates: the Bologna catalog (Battistini et al. 1987), the catalog by Magnier (1993), and the HST globular cluster candidate catalog (Barmby & Huchra 2001) – with search radius of $3''$. The expect that ~ 4 of our GC X-ray candidates could be spurious matches. The information on the properties of the X-ray sources and their optical identifications is shown in Table 3.

The X-ray images of M31 with GC X-ray source positions circled are shown in Fig. 2 and 3. The X-ray image shown in Fig. 2 was constructed combining the data of the *XMM-Newton*/EPIC-MOS1, MOS2 and pn cameras in the $0.3-7.0$ keV energy band. The X-ray image shown in Fig. 3 combines the data of *Chandra*/ACIS and HRC detectors.

4. NOTE ON THE EFFECT OF MULTIPLE UNRESOLVED X-RAY SOURCES

Recent *Chandra* observation of the Galactic globular cluster M15 has shown two distinct luminous X-ray sources separated by less than $3''$ (White & Angelini 2001). The spatial resolution of both *Chandra* ($\sim 0.5''$) and *XMM* ($\sim 10''$) is not sufficient to resolve most of possible multiple X-ray sources within one cluster in M31. Therefore, some of the M31 GC X-ray sources from our sample can be unresolved composites of separate sources (Angelini, Loewenstein & Mushotzky 2001; Di Stefano et al. 2002). It should thus be noted, that the spectral blending and superposition of variability of individual sources may complicate direct comparisons with Galactic globular cluster sources.

5. SPECTRAL PROPERTIES OF THE M31 GLOBULAR CLUSTER X-RAY SOURCES

Twenty seven and twenty three sources detected with *XMM-Newton* and *Chandra* have a sufficient number of counts to allow crude or detailed spectral modeling. Combining the above two samples gives us a high-quality information on the spectral properties of 31 bright GC X-ray sources. The representative spectra of bright GC sources obtained with *XMM-Newton*/EPIC and *Chandra*/ACIS are shown in Fig. 4.

The spectra of globular cluster candidates were fitted with a variety of spectral models using XSPEC v11. We first considered simple one-component spectral model: an absorbed simple power law. The results of fitting this model to the source spectra are given in Tables 4 and 5. The spectra of all these objects can be generally described by an absorbed simple power law model with photon index of $\sim 0.8-2.8$ and an equivalent absorbing column of $\sim (0.4-7.5)\times 10^{21}$ cm^{-2} (Table 4,5). The corresponding

isotropic luminosities of the globular cluster sources differ by four orders of magnitude and fall between $\sim 10^{35}$ and $\sim 10^{39}$ ergs s^{-1} in the $0.3-10$ keV energy band, assuming a distance of 760 kpc.

In most cases, we obtained acceptable fits using a power law spectral model (Table 4,5). However, for almost all brighter sources, a complex spectral models are required. For several sources with high luminosities (sources ##22, 26, 32, 42, 43 in Table 3), the models with quasi-exponential cut-off at $\sim 2-8$ keV or two-component models describe the energy spectra significantly better than a simple power law. To approximate the spectra of these sources, we used an absorbed power law model with exponential cut-off (XSPEC CUTOFFPL model), a Comptonization model and a two-component models.

For the Comptonization model approximation, we used the XSPEC model COMPTT (Sunyaev & Titarchuk 1980, Titarchuk 1994, Titarchuk & Lyubarskij 1995). This model includes self-consistent calculation of the spectrum produced by the Comptonization of the soft photons in a hot plasma. It contains as free parameters the temperature of the Comptonizing electrons, kT_e, the plasma optical depth with respect to the electron scattering, τ and the temperature of the input Wien soft photon distribution, kT_0. A spherical geometry was assumed for the Comptonizing region.

A cut-off power law and a Comptonization models gave reasonably good fit to the spectra of all sources considered, and the results are shown in Table 6. The model parameters derived for the M31 GC X-ray sources resemble those observed for bright Galactic low mass X-ray binaries (White, Stella & Parmar 1988; Christian & Swank 1997; Church & Balucinska-Church 2001).

The spectra of many luminous Galactic LMXB are well fit with a two-component model consisting of a soft black body-like component which might represent emission from an optically thick accretion disk or from the neutron star surface, together with hard component which may be interpreted as emission from a corona-like structure or a boundary layer between the disk and a neutron star (White, Stella & Parmar 1988; Christian & Swank 1997; Sidoli et al. 2001). We used such two-component models to approximate spectra of the three brightest globular cluster sources showing spectral cut-off (sources ##22, 42, 43). and 32)

For the soft component we used multicolor disk-blackbody (XSPEC DISKBB)(Mitsuda et al. 1984) and a black body (XSPEC BBODYRAD) models. DISKBB model has two parameters, the effective radius, $r_{in}\sqrt{cosi}$, where r_{in} is the inner radius of the disk, i is the inclination angle of the disk and kT_{in} is the maximum color temperature of the disk. Although this model does not take into account the effects of electron scattering and uses simplified temperature profile in the accretion disk (Shakura & Sunyaev 1973), it has been found to give an adequate qualitative description to the spectra of accreting X-ray binaries (Mitsuda et al. 1984; White, Stella & Parmar 1988; Christian & Swank 1997). The BBODYRAD model has two parameters, the effective radius, r_{BB} and color temperature, kT_{BB}.

The hard spectral component can be adequately described by various phenomenological and physical models involving a break in the slope of the spectrum or quasi-exponential spectral cut-off at higher energies. For the sake of easier comparison with the results for the Galactic LMXB (White, Stella & Parmar 1988; Christian & Swank 1997; Church & Balucinska-Church 2001), we use a simple black body BBODYRAD (in combination with DISKBB as a soft component) and a simple power law (in combination with BBODYRAD as a soft component) to approximate hard component in the spectra of brightest GC sources in our sample. The results of two-component approximation of the spectra of GC X-ray sources are shown in Table 7.

The two-component models give a good fit to the spectra of the high-luminosity GC X-ray sources in our sample. The characteristic temperature of the soft spectral component ranges from 0.5 to 1.2 keV, and the average contribution of the soft spectral component to the total source luminosity is $\sim 30\%$. Interestingly, even in the case of brightest M31 GC sources with total isotropic luminosities exceeding Eddington limit for the $1.4M_{\odot}$ neutron star, the absorption-corrected luminosity of the soft spectral component never significantly exceeds that limit. In conclusion, the two-component approximation of the spectra of bright M31 GC sources gives spectral parameters consistent with high luminosity LMXBs hosting a neutron star (White, Stella & Parmar 1988; Christian & Swank 1997; Church & Balucinska-Church 2001).

5.1. *Spectral distribution of GC X-ray sources*

In order to characterize the overall spectral properties of the bright GC X-ray sources, we constructed a distribution of their spectral indices in the $0.3-7.0$ keV energy range using the model fits to both *XMM-Newton* and *Chandra* data with an absorbed simple power law (Fig. 5). For the sources with multiple spectral measurements, we used average values of the photon index. The main part of the distribution including 29 sources out of 31 spans a range of photon indices between ~ 1.4 and ~ 2.2, and has a clearly defined maximum at $\alpha \sim 1.6$ (Fig. 5). Excluding two extremely hard X-ray sources, gives the corresponding weighted mean value of the photon index 1.65 ± 0.01. This distribution is reminiscent of the spectral distribution of the X-ray sources in the central bulge of M31 (Shirey et al. 2001). The X-ray population of the central bulge of M31 is very likely to be dominated by bright LMXBs. Based on the similarity in the properties of M31 GC X-ray sources and their Galactic counterparts, we expect most of M31 GC X-ray sources to be LMXBs. Therefore the similarity between the spectral distributions of the central bulge of M31 and that of its GC X-ray sources is not surprising. Moreover, the peak of the M31 GC spectral index distribution coincides with the average value of the spectral photon index ($\alpha \sim 1.6$) derived for the LMXB populations in the nearby galaxies of different morphological type (Irwin, Athey & Bregman 2003). The spectral photon indices of the M31 GC X-ray sources in our sample were found to lie in the range, observed for the Galactic GC sources, in agreement with previous studies (Di Stefano et al. 2002).

5.2. *Hardness-luminosity diagram of GC X-ray sources*

We studied the relation between the hardness of the spectrum and luminosity of GC X-ray sources in our sample. In Fig. 6 the hardness of the spectrum of GC X-

ray sources expressed in terms of spectral photon index is shown as a function of their X-ray luminosity in the $0.3-10$ keV energy band. As it is clearly seen from Fig. 6, there are three groups of sources, occupying distinct regions in the hardness-luminosity diagram. The first group represents majority of the brightest X-ray sources with luminosities above $\sim 4\times10^{37}$ ergs s^{-1}. The objects in this group have relatively narrow range of photon indices with average value of 1.55, suggesting common spectral formation mechanism at high luminosities. The second group comprised of fainter sources, shows greater variety of photon indices ranging from ~ 1.4 to ~ 2.3. Based on the wide range of X-ray luminosities, this group could represent a mix of LMXBs in both low and high luminosity states (White, Stella & Parmar 1988). The third group consists of two objects with extremely hard spectra ($\alpha\sim0.6-0.8$). Both objects also have a more pronounced spectral cut-off than the rest of the GC sources (Table 6). In addition, one of the sources, the X-ray source #32 in the globular cluster Bo 158, shows regular X-ray dips, implying a system observed at high inclination angle (Trudolyubov et al. 2002b). The hardness-luminosity diagram of GC X-ray sources in our sample appears to be consistent with that of the central bulge (Shirey et al. 2001).

5.3. *Low energy absorption*

The unprecedented sensitivity of *XMM* and *Chandra* observations allows a reliable measurement of low energy absorption toward brighter sources in M31. Using the results of spectral fitting, we have been able to estimate the value of equivalent hydrogen absorbing column, $N_{\rm H}$ for 31 source in our sample. To make a homogeneous sample, we used the same simple spectral model to estimate $N_{\rm H}$ for all sources (an absorbed power law model). It should be noted, that the amount of low-energy absorption derived from spectral fitting sometimes depends strongly on the type of continuum model used to approximate X-ray spectrum (Table 4,6). The simple power law approximation does not take into account possible presence of an additional soft X-ray component leading to the underestimation of the absorbing column. The choice of a particular model for the soft X-ray component (i.e. black body vs. multicolor disk black body) or a hard spectral continuum (i.e. a Comptonization model vs. simple power law) introduces additional uncertainty in the value of $N_{\rm H}$.

Our analysis shows that for the large fraction of GC sources the derived value of $N_{\rm H}$ is either in excess or consistent with Galactic hydrogen column $N_{\rm H}^{Gal}\sim7\times10^{20}$ cm^{-2} in the direction of M31 (Dickey & Lockman 1990). In the first case, it is natural to assume that additional absorption could be due to interstellar matter outside our Galaxy (i.e. in M31 and intergalactic medium) and/or within the X-ray binary itself. We compared the values of $N_{\rm H}$, derived from our spectral fits with values predicted using the optical observations. If there is no extra absorption within the X-ray binary itself, a close agreement between the absorbing column values derived from analysis of X-ray and optical data is expected (Sidoli et al. 2001).

Using the results of optical observations of M31 globular clusters (Barmby et al. 2000; Huchra, Brodie & Kent 1991; Perrett et al. 2002), we were able to estimate the values of optical extinction for 15 GC sources with measured X-ray low-energy absorption. The values of optical color excess, E_{B-V} were converted to the equivalent hydrogen column densities, $N_{\rm H}^{\rm opt}$ using the relation: $N_{\rm H}/E_{\rm B-V}=5.9\times10^{21}$ cm^{-2} mag^{-1} (Cox 2000). In Fig. 7 (*left panel*) the values of the X-ray low-energy absorption, $N_{\rm H}^{\rm X}$ are plotted against optically determined values, $N_{\rm H}^{\rm opt}$. The dotted line corresponds to equal X-ray and optically determined absorption. Taking the aforementioned systematic uncertainties in the derivation of X-ray absorption into account there is a general agreement between two absorption measurements (Fig. 7, *left panel*). Based on the current observations it is impossible to confirm or rule out a possibility of additional absorption in some sources. More sensitive observations with wider bandpass (i.e. future Constellation-X) and physically justified detailed spectral modeling are needed to resolve this interesting presently open issue.

The distribution of the X-ray absorption could provide additional information on the geometry of M31 globular cluster system and help to map the structure of ISM inside M31. For example, the sources located behind or inside the disk of M31 should be in general more absorbed/reddened than sources seen in front of the disk. We constructed the distribution of absorption columns for 31 M31 GC sources (Fig. 7, *right panel*). The distribution has a prominent peak centered at $\sim 1.2\times10^{21}$ cm^{-2} and a tail structure extending up to $\sim 6\times10^{21}$ cm^{-2}. In general, the observed $N_{\rm H}$ distribution could be consistent with homogeneous quasi-spherical spatial distribution of GC sources with an additional absorption from the disk.

6. VARIABILITY

6.1. *Long-term variability*

We searched for the long-term flux variability of M31 GC sources in our sample combining the data of multiple *Chandra* and *XMM-Newton* observations. We found that more than 80% of sources with multiple flux measurements available show significant variability (Table 3). In Fig. 8 the long-term flux histories of ten M31 GC sources demonstrating the highest levels of variability are shown. These sources show both irregular and possible quasi-periodic patterns of X-ray variability with corresponding flux changes by more than a factor of 2 over a time scales of several days to years.

The persistent low luminosity GC X-ray sources with average luminosities below $few\times10^{37}$ ergs s^{-1} tend to be generally more variable than brighter ones. The corresponding ratio between the highest and the lowest flux levels observed with *XMM* and *Chandra* is between ~ 3 and >15 for low luminosity sources, while it is usually lower than ~ 3 for the high luminosity sources.

The X-ray source associated with globular cluster Bo 107 shows a possible pattern of recurrent outbursts lasting for $\sim 50-100$ days spaced by $\sim 100-200$ day intervals. The source X-ray flux during the peak of the outburst can be at least ~ 10 times higher than during the low luminosity periods. This type of variability is reminiscent of the Galactic LMXB like Aql X-1 (Priedhorsky & Terrell 1984).

Di Stefano et al. (2002) proposed that the X-ray source in Bo 86 may have long-term periodicity on a time scale of $\sim$ 200 days (see also Kong et al. 2002). Our data, though covering a longer period of time, does not allow us

to confirm or completely rule out that kind of variability of Bo 86. More frequent observations would be needed to establish variability of the source.

We also searched for the long-term spectral variability of all bright M31 GC sources using the results of spectral analysis of *XMM* and *Chandra* data. Several sources demonstrate a correlation between the level of X-ray flux and hardness of their energy spectrum. The spectral fits for most of variable sources indicate that as the source flux increases, the spectrum becomes harder (Table 4). Two characteristic examples of such behavior are shown in Fig. 10 (sources Bo 78 and Bo 148). In this figure the hardness of X-ray spectrum expressed in terms of best-fit photon index is shown as a function of the source luminosity. The luminosity of the spectrally variable sources ranges from $\sim 10^{36}$ to $\sim few \times 10^{38}$ ergs s^{-1}, falling into typical range of luminosities for both atoll and Z-source classes of Galactic LMXB (Hasinger & van der Klis 1989). For brighter sources with luminosities around 10^{38} ergs s^{-1} the observed spectral changes could be consistent with that of the Z-sources on the normal branch (Hasinger & van der Klis 1989).

6.2. *Recurrent transient activity of Bo 163.*

One of the sources, coincident with a globular cluster Bo 163 shows a recurrent transient-like variability. Our analysis of the archival *Chandra* data revealed the presence of a bright X-ray source CXO J004317.8+412745 with a position consistent with Bo 163 and previously detected *ROSAT* source RX J0043.2+4127 (Supper et al. 2001) during 2001 February 18 ACIS-S observation (Obs. ID #1582) (Fig. 9, *upper panel*). The estimated X-ray luminosity of the source was $\sim 10^{38}$ ergs s^{-1} in the $0.3-10$ keV energy band (see source spectral parameters in Table 5). Other *XMM-Newton* and *Chandra* observations covering the position of Bo 163 did not yield positive source detection with 2σ upper limits on its luminosity ranging from $\sim 10^{35}$ to $\sim 10^{37}$ ergs s^{-1} (depending on the type of instrument and exposure time).

We analyzed the data of the earlier observations of Bo 163/RX J0043.2+4127 with *ROSAT*/PSPC and HRI detectors. The observed *ROSAT* source count rates were converted into the X-ray fluxes in the $0.3-10$ keV energy band using WebPIMMS assuming an absorbed power law spectrum with $N_{\rm H} = 7 \times 10^{20}$ cm^{-2} and $\alpha = 1.7$. The resulting *ROSAT* light curve of RX J0043.2+4127 is shown in *lower panel* of Fig. 9. The source clearly demonstrates a pattern of recurrent transient-like behavior with bright outbursts with $L_{\rm X} > 10^{38}$ ergs s^{-1} and an extended quiescent periods with $L_{\rm X} < 10^{36}$ ergs s^{-1}. The corresponding maximum ratio of the the highest outburst luminosity ($L_{\rm X} \sim 2 \times 10^{38}$ ergs s^{-1}) to the lowest measured quiescent luminosity ($L_{\rm X} < 10^{35}$ ergs s^{-1}) is > 2000.

The overall X-ray properties of RX J0043.2+4127 are reminiscent of both Galactic neutron star and black hole recurrent transients like Cen X-4 (Kaluzienski, Holt & Swank 1980, van Paradijs et al. 1987) and 4U1630-40 (Priedhorsky 1986). Unfortunately, current spectral and timing data does not allow us to determine the nature of the compact object in RX J0043.2+4127. Observations with higher sensitivity and timing resolution are needed to choose between neutron star and black hole interpretation.

6.3. *Short-term variability.*

The comparisons based on the broad-band spectral properties are not sufficient to establish a neutron star nature or rule out a black hole nature for the M31 globular cluster sources. On the other hand, the study of their short-term variability can provide a definitive answer, if Type I X-ray bursts or X-ray pulsations are observed. We searched for both types of variability in the M31 GC data. Unfortunately, the observed source count rates for most sources are too low to allow us to probe timescales shorter than $\sim 20-30$ seconds. We did not find evidence of X-ray pulsations and short X-ray bursts in the *XMM-Newton* and *Chandra* data.

Several GC sources demonstrate significant aperiodic variability on a time scale of individual observation. As an example of such behavior, the lightcurves of three GC sources are shown in Fig. 11. All three sources (Bo 86, Bo 107 and Bo 135) show irregular changes of X-ray flux of up to $\sim 100\%$ over a time scales of $1000-10000$ s. These sources were also found to be variable on a time scales of months to years (Fig. 8). The combination of such short and long term variabilities was long recognized as one of the characteristic features of X-ray binaries (Hasinger & van der Klis 1989). In addition, the X-ray source coincident with M31 GC candidate Bo 158 shows a remarkable dip-like modulation with a a period of 10017 s (Trudolyubov et al. 2002b).

The unprecedented sensitivity of *XMM-Newton* provides a unique opportunity to study spectral evolution of the brightest LMXB sources in M31 on a time scale of hundreds and thousands of seconds. To study short-term spectral variability of the bright GC sources, we constructed their X-ray hardness-intensity diagrams using the data of *XMM-Newton* observations. The X-ray hardness was defined as the ratio of the source intensities in the $2.0-7.0$ keV and $0.3-2$ keV energy bands with data integration times of $1000-3000$ s depending on the source intensity. Several sources show a complex patterns of evolution on the hardness-intensity diagram somewhat reminiscent of the Galactic Z and atoll sources (Hasinger & van der Klis 1989). In Fig. 12, we show the hardness-intensity diagram of one of these sources, the X-ray source in globular cluster Bo 148. Although the data strongly suggest some pattern of spectral evolution, it is still insufficient to classify source behavior in conventional framework of Galactic LMXB. More high-sensitivity observations covering wider range of source luminosities are needed to address this issue.

6.4. *"Dipping" X-ray source in Bo 158*

The X-ray source J004314.1+410724 was discovered in M31 by the *Einstein* observatory (source #85 in Trinchieri & Fabbiano 1991) and was detected in subsequent observations with *ROSAT* (Primini et al. 1993, Supper et al. 2001), *XMM-Newton* (Trudolyubov et al. 2002b) and *Chandra* (Di Stefano et al. 2002). The position of the source is consistent with the optically identified globular cluster candidate Bo 158 (source #158 in Table IV of Battistini et al. 1987). The observation of the central bulge of M31 with *XMM-Newton* taken 2002 Jan 6 revealed strong periodic dip-like modulation of the source flux (Trudolyubov et al. 2002b; Fig. 13, *upper panel*). The

X-ray flux was modulated by $\sim 83\%$ at a period of 2.78 hr (10017 s). The X-ray intensity dips show no energy dependence. The analysis of earlier archival *XMM* and *ROSAT* observations taken in the year 2000 and 1991 revealed weaker dips with amplitudes of $\sim 30\%$ and $\sim 50\%$. The amplitude of the modulation has been found to be anticorrelated with source X-ray flux. A detailed description of the timing and spectral properties of Bo 158 are presented in Trudolyubov et al. 2002*b*.

We extended our original study of the X-ray modulation in Bo 158 combining the data of archival *XMM* and *Chandra* observations. Because of a relatively long period of modulation (~ 10000 s), only one *Chandra* observation was selected for our analysis (Obs. #2017 with ACIS). For one *XMM* observation (Obs. #1), showing significant change of the source flux on a time scale of ~ 5 hours, we divided the data into two segments corresponding to different luminosity levels. A sample light curves of Bo 158 obtained with *XMM* and *Chandra* are shown in the upper and middle panels of Fig. 13. The modulation fraction (i.e. the ratio of the average modulation amplitude to the average source flux) was determined for each observation. The resulting dependence of the modulation fraction on the source flux is shown in the bottom panel of Fig. 13. The relative amplitude of X-ray modulation declines dramatically (at least by factor of ~ 10) as the source luminosity rises from $\sim 4.5 \times 10^{37}$ to $\sim 1.4 \times 10^{38}$ ergs s^{-1}. The observed correlation between the modulation fraction and X-ray flux of Bo 158 allows us to put constraint on possible number of bright X-ray sources presently active in this cluster. We conclude that one X-ray source must contribute up to 99% of the detected flux.

In addition to the short-term periodic variability, there is clear evidence for significant long-term variability of Bo 158. The long-term monitoring observations with *Chandra* and *XMM-Newton* (Fig. 8) show that the source is highly variable on a time scales of months to years. The X-ray luminosity Bo 158 changes at least by factor of ~ 4, e.g. between $\sim 5 \times 10^{37}$ and $\sim 2 \times 10^{38}$ ergs s^{-1}.

7. LUMINOSITY DISTRIBUTION OF M31 GC X-RAY SOURCES.

We have built differential and cumulative luminosity distributions of M31 GC X-ray sources assuming a distance of 760 kpc (Fig. 14). The luminosity distribution for the central bulge based on the results of *XMM-Newton* observations (Trudolyubov et al. 2002*a*) is also shown in Fig. 14. Luminosities of the brighter sources ($L_{\rm X} > 5 \times 10^{36}$ ergs s^{-1}) were derived using analytical fits to their spectra in the $0.3 - 10$ keV energy band. For faint sources, luminosities were derived using WebPIMMS, assuming an absorbed power law model with $N_{\rm H} = 7 \times 10^{20}$ cm^{-2} (Dickey & Lockman 1990) and $\alpha = 1.7$ (Shirey et al. 2001) in the same energy band. For sources with multiple flux measurements available, we used average flux to calculate the luminosity. Taking into account the sensitivity as a function of off-axis distance, different exposure times and the effect of diffuse X-ray emission near the center of M31, we estimate flux completeness limit of our samples as $\sim 10^{36}$ ergs s^{-1} (indicated by dotted line in Fig. 14).

The shapes of both cumulative and differential luminosity distributions for M31 GC sources indicate the presence of a cut-off and can be described by a broken power law or a cut-off power law models. We fitted the cumulative luminosity distribution with two power laws at luminosities below and above 5×10^{37} ergs s^{-1}. For source luminosities between 10^{36} and 5×10^{37} ergs s^{-1}, we obtain the slope of -0.3 ± 0.1 with normalization of 38 sources at 10^{36} ergs s^{-1}, for higher luminosities, the integral slope is $-1.2^{+0.4}_{-0.7}$ (shown as dotted lines in Fig. 14). We also fitted the unbinned differential luminosity with a power law with exponential cut-off: $L^{-\alpha}\exp(-L/L_{\rm cut})$. The resulting values of α and the cut-off luminosity are 1.0 and $2.7^{+4.3}_{-0.9} \times 10^{38}$ ergs s^{-1} respectively. There is some flattening of the cumulative distribution toward the faint luminosity end, probably caused by incompleteness of our sample.

As it is clearly seen from Fig. 14, the integrated luminosity function of GC sources differs significantly from that of the other point sources in the central bulge of M31. The low luminosity part of the GC luminosity distribution is somewhat flatter than that of the central bulge of M31. The luminosity of the break in the slope of the luminosity function appears to be $\sim 2 - 3$ times higher for GC sources ($L_{\rm br}^{\rm GC} \sim 5 \times 10^{37}$ ergs s^{-1}) than for the sources in the central bulge with $L_{\rm br}^{\rm bulge} \sim (1.5 - 2.0) \times 10^{37}$ ergs s^{-1} (Shirey et al. 2001, Trudolyubov et al. 2002a, Kong et al. 2002*a*). Qualitatively, the fraction of the bright sources ($L_{\rm X} > few \times 10^{37}$ ergs s^{-1}) is higher for the GC population than for the central bulge population. It is interesting to note that in spite of the aforementioned differences, the slopes of the high-luminosity parts of the luminosity distributions for the M31 GC and central bulge populations are very close to each other.

In addition, there is an obvious difference between the luminosity functions of GCs and X-ray sources in the disk of M31 (Trudolyubov et al. 2002a). The luminosity distribution of the disk X-ray source population terminates at much lower luminosities (*few* $\times 10^{37}$ ergs s^{-1}) (Trudolyubov et al. 2002a) than that of the M31 GCs (*several* $\times 10^{38}$ ergs s^{-1}).

It is also interesting to compare the luminosity functions of the Galactic GC and M31 GC X-ray sources. These two functions have two main differences: i) the peak X-ray luminosity of the M31 GC X-ray sources is ~ 10 times higher than that of the brightest Galactic GC X-ray source (Di Stefano et al. 2002); ii) the fraction of the bright sources is much higher for the M31 GC population than for the Galactic GC population; 13 sources or $\sim 30\%$ of the total number of GC sources detected in our survey reached luminosity of 5×10^{37} ergs s^{-1}, while only one Galactic GC source, X1820-303 (NGC 6624) has luminosity occasionally exceeding this level (Sidoli et al. 2001).

8. ON THE ROLE OF THE BRIGHT GC SOURCES IN THE X-RAY SOURCE POPULATION OF M31.

We found that $\sim 10\%$ of the optically identified GC candidates in the regions of M31, covered by *XMM-Newton* and *Chandra* observations, harbor bright X-ray sources with luminosities above 10^{35} ergs s^{-1} (43 X-ray sources were found among ~ 400 GC candidates). This fraction is comparable to the observed for the Milky Way globular cluster system with 14 bright X-ray sources among known 150 globular clusters (Verbunt et al. 1995, Sidoli et al. 2001, Harris 1996). In addition, the fraction of M31 GCs that contain X-ray sources with luminosities above

$\sim 10^{37}$ ergs s^{-1} ($\sim 5\%$) appears to be consistent with that derived for a large sample of galaxies of various morphological types (Sarazin et al. 2003).

Our observations clearly indicate that GC X-ray sources make dominant contribution to the bright ($L_X > few \times 10^{37}$ ergs s^{-1}) source counts in the surveyed areas of M31. Six persistent globular cluster X-ray sources (sources $\#\#2, 9, 22, 41, 42, 43$) have absorbed luminosities in the $0.3 - 10$ keV energy band exceeding 10^{38} ergs s^{-1}; three other persistent GC sources in our sample (sources $\#\#31, 32, 37$) occasionally exceed that luminosity level, i.e. at least six GC X-ray sources are brighter than 10^{38} ergs s^{-1} at any given time. Apart from transient X-ray sources, we detected only one persistent non-GC source belonging to M31, having average luminosity in excess of 10^{38} ergs s^{-1}, RX J0042.6+4115 (Barnard, Kolb & Osborne 2003), and two other non-GC sources occasionally exceeding that luminosity level in the same regions. Therefore, from $\sim 67\%$ to $\sim 90\%$ of the sources brighter than 10^{38} ergs s^{-1} observed in the surveyed area at any given time are associated with globular clusters. According to the results of our survey, about 20 sources or $\sim 40\%$ of the total number of sources with luminosities above 10^{37} ergs s^{-1} detected in *XMM* and *Chandra* observations of M31, reside in globular clusters.

We found that fraction of bright X-ray sources ($L_X > 10^{37}$ ergs s^{-1}), residing in globular clusters is significantly higher in M31 ($\sim 40\%$) than in Milky Way Galaxy ($\sim 5 - 10\%$) (Liu et al. 2001). It should be also noted, that no persistent GC sources with luminosities in excess of 10^{38} ergs s^{-1} have been detected in our Galaxy so far, compared to six sources found in M31. On the other hand, the fraction of bright GC X-ray sources in M31 is surprisingly similar to the observed in early-type galaxies: i.e. NGC 1399 (Angelini, Loewenstein & Mushotzky 2001) and NGC 4472 (Kundu, Maccarone, & Zepf 2002).

9. SPATIAL DISTRIBUTION AND LUMINOSITY OF M31 GC X-RAY SOURCES.

The spatial distribution of GC X-ray sources detected with *XMM-Netwon* and *Chandra* is shown in Fig. 15. We have noticed that bright X-ray sources tend to reside at significantly larger galactocentric distances than the fainter sources. In fact, all GC X-ray sources with luminosities steadily exceeding 10^{38} ergs s^{-1} (shown in Fig. 15 with *large white circles*) happen to have angular distances more than $15'$ from the center of the galaxy, or well outside the central bulge of M31, where the most of fainter GC X-ray sources are residing.

10. ON THE CORRELATION BETWEEN THE X-RAY AND OPTICAL PROPERTIES.

We used the results of optical observations of M31 GC candidates (Huchra, Brodie & Kent 1991; Barmby et al. 2000; Perrett et al. 2002) to study how the properties of the X-ray sources depend on the optical properties of the globular clusters hosting them.

We found that globular clusters hosting bright X-ray sources tend to be optically brighter than the rest of M31 globular clusters, in agreement with previous studies (Di Stefano et al. 2002). To illustrate this effect, V-magnitude distribution of X-ray bright globular clusters from our sample is shown in Fig. 16(*left panel*) along with the distribution for the whole sample of GC candidates from Battistini et al. (1987). Similar tendency for bright X-ray sources to be associated with more optically luminous GCs has been also observed in several early-type galaxies (Sarazin et al. 2003). Sarazin et al. (2003) shows that this tendency could be consistent with a constant probability of finding an LMXB per unit optical luminosity of the cluster.

Both Galactic and M31 globular clusters hosting bright LMXBs were found to be both denser and more metal-rich (Bellazzini et al. 1995). We studied the effect of globular cluster metallicity, [Fe/H] on the properties of the M31 GC X-ray sources from our sample. For 31 GC X-ray sources the results of metallicity measurements are available (Huchra, Brodie & Kent 1991; Barmby et al. 2000; Perrett et al. 2002). The metallicity distribution of the X-ray bright GC in our sample is shown in Fig. 16(*right panel*). The population of X-ray emitting GC yields a weighted mean $<$ [Fe/H] $>_{\rm XR} = -1.06 \pm 0.02$, significantly higher than $<$ [Fe/H] $>_{\rm nXR} = -1.37 \pm 0.01$ derived for the non-X-ray GC subsample from Perrett et al. (2002), in agreement with results of previous studies (Bellazzini et al. 1995). We used a Kolmogorov-Smirnov (KS) test to determine whether X-ray emitting GC and non-X-ray GC populations were drawn from the same distribution. The hypothesis that the two distributions are extracted from the same parent population can be rejected at the confidence level of $\sim 93\%$.

The dependence of the X-ray luminosity of M31 GC sources on the metallicity of their host globular clusters is shown in the *left panel* of Fig. 17. The data points can be separated into two main groups corresponding to the source X-ray luminosities below and above $\sim 10^{38}$ ergs s^{-1}. The first group (sources with X-ray luminosities below 10^{38} ergs s^{-1}) has weighted mean metallicity of -0.79 ± 0.04 and possibly demonstrates general tendency of the brighter sources to reside in the more metal rich clusters. This behavior could be consistent with possible correlation between X-ray luminosity and cluster metallicity found by Sidoli et al. (2001) for the sample of bright Galactic GC sources. It is also interesting to note, that all known Galactic GC X-ray sources have luminosities in the range occupied by the first group (Sidoli et al. 2001). The whole second group (sources with X-ray luminosities above 10^{38} ergs s^{-1}) occupies low metallicity region with weighted mean metallicity of -1.12 ± 0.02.

Recent X-ray observations and theoretical work suggest that spectral hardness of the bright LMXB sources in the soft X-ray band ($0.1 - 2.4$ keV) can depend on the average metallicity of the globular clusters harboring them. The soft X-ray spectra of the sources located in the metal-poor GCs were found to be harder than those of the metal-rich clusters (Irwin & Bregman 1999; Maccarone, Kundu & Zepf 2004). To demonstrate the effect of cluster metallicity on the intrinsic spectral hardness of the M31 GC X-ray sources, in the *right panel* of Fig. 17 the spectral power law photon index in the $0.3 - 7$ keV energy band for the GC sources from our sample is shown as a function of metallicity of the globular clusters hosting them. As it is seen from Fig. 17 (*right panel*), there is a possible correlation of the X-ray spectral hardness and the metallicity. We note however, that it is premature to draw any conclusions on the relationship between the intrinsic spectral

parameters of X-ray sources and metallicity of their host clusters, based on a model-dependent presentation of the spectrum measured in the narrow energy band. For example, using a multi-component spectral modeling of the *BeppoSAX* broad-band data for the bright Galactic GC sources, Sidoli et al. (2001) found a correlation between the temperature of the soft spectral component and a cluster metallicity, opposite to the results obtained in the soft X-ray band with one-component spectral models (Irwin & Bregman 1999).

11. ON THE NATURE OF M31 GC X-RAY SOURCES

Several GC X-ray sources observed in M31 have luminosities exceeding 10^{38} ergs s^{-1}, being much brighter than any of the Galactic GC X-ray sources (Table 3). Four X-ray sources in our sample (##$2, 10, 22, 42$) have luminosities close to or exceeding a formal Eddington limit for the $1.4M_{\odot}$ neutron star. Nevertheless, such a high luminosities are not uncommon for bright low-mass X-ray binaries containing neutron star primaries. The Z-source subclass of Galactic LMXB is characterized by high X-ray luminosities ($> 10^{38}$ ergs s^{-1}) (Hasinger & van der Klis 1989) with two sources, Sco X-1 and GX 5-1, regularly exceeding Eddington limit for a neutron star (Liu et al. 2001). Recently, Barnard, Kolb and Osborne (2003) found that bright M31 X-ray source, RX J0042.6+4115 with extremely high X-ray luminosity of $\sim 5{\times}10^{38}$ ergs s^{-1} could be also classified as a neutron star Z-source. On the other hand, among stellar mass black hole X-ray sources, only transients in outburst (Chen, Shrader & Livio 1997) and highly variable systems like GRS 1915+105 (Morgan, Remillard & Greiner 1997) reach luminosities observed for bright M31 GC sources.

All bright X-ray sources found in the Milky Way globular clusters show Type I X-ray bursts and probably contain neutron star primaries. Moreover, theoretical calculations predict the probability of finding a black hole X-ray binary in the globular cluster to be much smaller than the neutron star binary due to dynamical effects and extremely low duty cycles of black hole binaries (Kulkarni et al. 1993, Sigurdsson & Hernquist 1993, Kalogera, King & Rasio 2004). The considerations mentioned above, and a general similarity between the M31 and Milky Way globular cluster systems allow us to expect most of the persistent M31 GC X-ray sources to be LMXB systems containing a neutron star primaries. However, the possibility of finding an active accreting black holes in our GC source sample can not be ruled out, based on the current spectral and timing data. For example, the X-ray source RX J0043.2+4127 associated with globular cluster Bo 163 shows a pattern of recurrent transient outbursts and quiescent periods (Fig. 9) typical for both neutron star and black hole transient systems. The study of short-term variability of GC X-ray sources in M31 with future missions can provide a definitive answer, if Type I X-ray bursts or X-ray pulsations are observed from these objects. The broad-band long-term monitoring of the transient/highly variable GC sources could also provide valuable information on their spectral evolution helping to establish the nature of these systems.

Some of the M31 GC X-ray sources in our sample might be unresolved composites of separate sources (Angelini, Loewenstein & Mushotzky 2001; Di Stefano et al. 2002). Recent high-resolution *Chandra* observations of the Galactic globular clusters revealed that one of the bright Galactic GC sources is a composite of two X-ray sources of comparable brightness (White & Angelini 2001). Depending on the probability of finding a bright X-ray source in a GC, we can expect to find $2-4$ GC X-ray sources in our sample (or $\sim 5-10\%$ of the total number) to be composites of two independent sources (Di Stefano et al. 2002).

12. SUMMARY

Utilizing the data of *XMM-Newton* and *Chandra* observations, we performed a study of individual and group properties of 43 X-ray sources identified with globular clusters in M31. The correlation between the optical parameters of the host globular clusters and the properties of X-ray sources associated with them was also studied. We compare the individual and group properties of M31 GC X-ray sources with the properties of their Galactic counterparts.

The spectral properties of the bright GC X-ray sources in our sample were found to be similar to that of the LMXB located in the bulge and globular clusters of the Milky Way Galaxy at the same luminosity levels (White, Stella & Parmar 1988; Christian & Swank 1997; Church & Balucinska-Church 2001). We note, that some GC sources could be unresolved composites of two or even more sources of comparable brightness complicating direct comparison with their Galactic counterparts. For the majority of sources, we obtained acceptable fits using a power law spectral model approximation. However, for several sources with high luminosities, the models with quasi-exponential cut-off at $\sim 2-8$ keV or two-component models describe the energy spectra significantly better than a simple power law. Several sources demonstrate a correlation between the level of X-ray flux and hardness of their energy spectrum similar to the Galactic Z and atoll-sources (Hasinger & van der Klis 1989). The spectral distribution of M31 GC X-ray sources resembles the corresponding distributions derived for the the central bulge of M31 (Shirey et al. 2001) and other nearby galaxies of different morphological type (Irwin, Athey & Bregman 2003).

There is no evidence that X-ray variability of M31 GC sources and bright Galactic LMXB (both GC and non-GC) differ. We found that $\sim 80\%$ of the sources in our sample with multiple flux measurements available show significant variability on a time scales from days to years. We note, that in some GC X-ray sources the observed variability could be result of superposition of flux variations of several unresolved sources. The X-ray source RX J0043.2+4127 in Bo 163 has been found to show recurrent transient outbursts with peak luminosities above 10^{38} ergs s^{-1}, typical for Galactic recurrent transients that harbor both neutron stars and black holes. Several sources show significant variability on a time scale of individual observations, ranging from aperiodic fluctuations to regular dipping (Bo 158).

The X-ray luminosity function of GC sources is found to be significantly different from that of the other point sources in the bulge and disk of M31 and Galactic GC X-ray sources. The luminosity distributions of the GC X-ray sources in M31 and that of the Milky Way have two main differences: i) the peak luminosity of the M31 GC X-ray sources is ~ 10 times higher than that of the brightest Galactic GC X-ray source; ii) the fraction of the bright

sources is much higher for the M31 GC population; $\sim 30\%$ of the GC sources detected in our survey reached the luminosity of 5×10^{37} ergs s^{-1}, while only one of 14 Galactic GC sources, X1820-303 (NGC 6624) has luminosity occasionally exceeding this level (Sidoli et al. 2001).

We found that $\sim 10\%$ of the optically identified GC candidates in the regions of M31, covered by *XMM-Newton* and *Chandra* observations, harbor bright X-ray sources with luminosities above 10^{35} ergs s^{-1}. This fraction is comparable to that observed for the Milky Way globular cluster system with 14 bright X-ray sources among known $\sim$ 150 globular clusters (Verbunt et al. 1995, Sidoli et al. 2001, Harris 1996). In addition, the fraction of M31 GCs that contain X-ray sources with luminosities above $\sim 10^{37}$ ergs s^{-1} ($\sim 5\%$) appears to be consistent with that derived for a large sample of galaxies of different morphological type (Sarazin et al. 2003).

The inferred isotropic X-ray luminosities of the GC sources lie between $\sim 10^{35}$ and $\sim 10^{39}$ erg s^{-1} in the $0.3-10$ keV energy band. Six persistent sources (or $\sim 14\%$ of the total number) have luminosities steadily exceeding 10^{38} erg s^{-1}, and three other sources occasionally exceed that luminosity level. Four X-ray sources in our sample (##2, 10, 22, 42) have luminosities close to or exceeding the Eddington limit for the $1.4M_{\odot}$ neutron star. Our observations indicate that GC sources make dominant contribution to the bright source counts in the areas of M31 covered by the survey: $\sim 40\%$ of the total number of sources with luminosities above 10^{37} ergs s^{-1} reside in GCs. The fraction of the GC X-ray sources rises to $67-90\%$ if one considers source luminosities above 10^{38} erg s^{-1}. The contribution of the GC sources to the total number of bright sources found in M31 is much higher (by factor of > 4) than in the Milky Way galaxy. On the other hand, there is a surprising similarity between the fractions of bright GC X-ray sources in M31 and in the early-type galaxies (Angelini, Loewenstein & Mushotzky 2001, Kundu, Maccarone, & Zepf 2002).

The distribution of radial distances of GC X-ray sources from the center of M31 shows that brightest systems with luminosities steadily exceeding 10^{38} erg s^{-1} reside at greater galactocentric distances than the rest of the GC sources.

We used the results of optical observations of M31 GC candidates to study how the properties of the X-ray sources depend on the optical properties of the globular clusters hosting them. We found that globular clusters hosting bright X-ray sources tend to be optically brighter and more metal rich than the rest of M31 globular clusters, in agreement with previous studies (Bellazzini et al. 1995, Di Stefano et al. 2002). The comparison of the X-ray properties of GC sources with metallicity of their host globular clusters has shown that the brightest sources with luminosities above $\sim 10^{38}$ ergs s^{-1} tend to reside in more metal poor clusters than the fainter sources.

The remarkable similarities between the properties of the M31 GC X-ray sources and that of the Galactic neutron star LMXBs allow us expect most of the persistent M31 GC X-ray sources to be LMXB systems with neutron star primaries. We note, however, that current X-ray spectral and timing data can not rule out the possibility of finding an active accreting black holes in our GC source sample. The study of short-term variability and broad-band spectral evolution of GC X-ray sources in M31 with future missions can provide valuable information allowing to establish the nature of these systems.

In conclusion, we note that in spite of the similarities of the spectral shape and variability patterns of individual M31 GC X-ray sources and Galactic LMXBs (both GC and non-GC), the group properties of M31 and Milky Way globular cluster X-ray sources differ significantly. The M31 GC source population has a much higher fraction of bright X-ray sources and higher peak luminosity than the Milky Way GC population, probably suggesting different formation histories and evolution. The large fraction of GC systems among the bright X-ray sources in M31 makes the M31 population of GC X-ray sources more like giant early-type galaxies than the Milky Way.

13. ACKNOWLEDGMENTS

Part of this work was done during a summer workshop at the Aspen Center for Physics, authors are grateful to the Center for their hospitality. Support for this work was provided through NASA Grant NAG5-12390. This research has made use of data obtained through the *Chandra* public data archive. *XMM-Newton* is an ESA Science Mission with instruments and contributions directly funded by ESA Member states and the USA (NASA). This research has made use of data obtained through the High Energy Astrophysics Science Archive Research Center Online Service, provided by the NASA/Goddard Space Flight Center.

REFERENCES

Anders, E., & Grevesse, N. 1989, Geochim. Cosmochim. Acta, 53, 197
Angelini, L., Loewenstein, M., & Mushotzky, R. 2001, ApJ, 557, L35
Arnaud, K. 1996, in Astronomical Data Analysis Software and Systems V, ASP Conference Series 101, ed. G. Jacoby & J. Barnes (San Francisco: ASP) 17
Barmby, P., Huchra, J.P., Brodie, J.P., Forbes, D.A., Schroder, L.L., & Grillmar, C.J. 2000, AJ, 119, 727
Barmby, P., & Huchra, J.P. 2001, ApJ, 122, 2458
Barnard, R., Kolb, U., & Osborne, J. P. 2003, A&A, 411, 553
Battistini, P., et al., 1987, A&AS, 67, 447
Bellazzini, M., Pasquali, A., Federici, L., Ferraro, F. R., & Fusi Pecci, F. 1995, ApJ, 439, 687
Chen, W., Shrader, C. R., & Livio, M. 1997, ApJ, 491, 312
Church, M. J., & Balucinska-Church, M. 2001, A&A, 369, 915
Christian, D. J., & Swank, J. H. 1997, ApJS, 109, 177
Clark, G. W. 1975, ApJ, 199, L143
Cox, A. N. 2000, in Allen's Astrophysical Quantities, ed. A. N. Cox, fourth edition, AIP Press
Davis, J. E. 2001, ApJ, 562, 575
Davis, J. E. 2003, http://space.mit.edu/CXC/analysis/davis/head2002/
Di Stefano, R., Kong, A. K. H., Garcia, M. R., Barmby, P., Greiner, J., Murray, S. S., & Primini, F. A. 2002, ApJ, 570, 618
Dickey, J. M., & Lockman F. J. 1990, ARA&A, 28, 215
Fabian, A. C., Pringle, J. E., & Rees, N. J. 1975, MNRAS, 172, 15P
Garcia, M. R., Murray, S. S., Primini, F. A., Forman, W., McClintock, J., & Jones, C. 2000, ApJ, 537, L23
Hasinger, G., & van der Klis, M. 1989, A&A, 225, 79
Harris, W. E. 1996, AJ, 112, 1487
Hertz, P., & Grindlay, J. E. 1983, ApJ, 275, 105
Huchra, J.P., Brodie, J.P., & Kent, S.M. 1991, ApJ, 370, 495
Irwin, J. A., & Bregman, J. N. 1998, ApJ, 510, L21
Irwin, J. A., Athey, A. E., & Bregman, J. N. 2003, ApJ, 587, 356
Kaaret, P. 2002, ApJ, 578, 114

Kalogera, V., King, A. R., & Rasio, F. A. 2004, ApJ, in press (astro-ph/0308485)
Kaluzienski, L. J., Holt, S. S., & Swank, J. H. 1980, ApJ, 241, 779
Kong, A. K. H., Garcia, M. R., Primini, F. A., Murray, S. S., Di Stefano, R., & McClintock, J. E. 2002*a*, 577, 738
Kulkarni, S., Hut, P., & McMillan, S. 1993, Nature, 364, 421
Kundu, A., Maccarone, T. J., & Zepf, S. E. 2002, ApJ, 574, L5
Liu, Q. Z., van Paradijs, J., & van den Heuvel, E. P. J. 2001, A&A, 368, 1021
Long, R. S., & van Speybroek, L. P. 1983, in Accretion-driven Stellar X-ray Sources (A84-35577-90), ed. W. H. G. Lewin & E. P. J. van den Heuvel (Cambridge: Cambridge Univ. Press), 117
Maccarone, T. J., Kundu, A., & Zepf, S. E. 2004, ApJ, submitted (astro-ph/0401333)
Magnier, E. 1993, Ph.D. thesis, MIT
Mitsuda, K., Inoue, H., Koyama, K., et al. 1984, PASJ, 36, 741
Morgan, E. H., Remillard, R. A., & Greiner, J. 1997, ApJ, 482, 993
van Paradijs, J., Verbunt, F., Shafer, R. A., & Arnaud, K. A. 1987, A&A, 182, 47
Perrett, K.M., Bridges, T.J., Hanes, D.A., Irwin, M.J., Brodie, J.P., Carter, D., Huchra, J.P., & Watson, F.G. 2002, AJ, 123, 2490
Priedhorsky. W. C., & Terrell, J. 1984, ApJ, 280, 661
Priedhorsky, W. 1986, A&SS, 126, 89
Primini, F. A., Forman, W., & Jones, C., 1993, ApJ, 410, 615
Sarazin, C. L., Kundu, A., Irwin, J. A., Sivakoff, G. R., Blanton, E. L., & Randall, S. W. 2003, ApJ, 595, 743
Shirey, R., Soria, R., Borozdin, K., Osborne, J. P., Tiengo, A., Guainazzi, M., Hayter, C., La Palombara, N., Mason, K., Molendi, S., Paerels, F., Pietsch, W., Priedhorsky, W., Read, A. M., Watson, M. G., West, R. G., 2001, A&A, 365, L195
Sidoli, L., Parmar, A. N., Oosterbroek, T., Stella, L., Verbunt, F., Masetti, N., & Dal Fiume, D., 2001, A&A, 368, 451
Sigurdsson, S., & Hernquist, L. 1993, Nature, 364, 423
Strueder, L. et al., 2001, A&A, L18
Shakura, N. I., & Sunyaev, R. A. 1973, A&A, 24, 337
Sunyaev, R. A., & Titarchuk, L. G. 1980, A&A, 86, 121
Supper, R., Hasinger, G., Pietsch, W., Truemper, J., Jain, A., Magnier, E.A., Lewin, W.H.G., & van Paradijs, J. 1997, A&A, 317, 328
Supper, R., Hasinger, G., Lewin, W. H. G., Magnier, E.A., van Paradijs, J., Pietsch, W., Read, A.M., & Truemper, J. 2001, A&A, 373, 63
Titarchuk, L. 1994, ApJ, 434, 570
Titarchuk, L., & Lyubarskij, Y. 1995, ApJ, 450, 876
Trinchieri, G., & Fabbiano, G., 1991, ApJ, 382, 82
Trudolyubov, S., Borozdin, K., & Priedhorsky, W. 2001, ApJ, 563, L119
Trudolyubov, S., Borozdin, K., & Priedhorsky, W., Mason, K., & Cordova, F. 2002a, ApJ, 571, L17
Trudolyubov, S., Borozdin, K., & Priedhorsky, W., Osborne, J., Watson, M., Mason, K., & Cordova, F. 2002b, ApJ, 581, L27
Turner, M. et al., 2001, A&A, 365, L27
van den Bergh, S. 2000, The Galaxies of the Local Group, (Cambridge: Cambrdge Univ. Press)
Verbunt, F., Bunk, W., Hasinger, G., & Johnston, H. 1995, A&A, 300, 732
White, N. E., Stella, L., & Parmar, A. N. 1988, ApJ, 324, 363
White, N. E., & Angelini, L. 2001, ApJ, 561, L101

TABLE 1

XMM-Newton OBSERVATIONS OF M31 FIELDS USED IN OUR ANALYSIS.

Obs. #	Date, UT	Field	Obs. ID	RA (J2000)[a] (h:m:s)	Dec (J2000)[a] (d:m:s)	Exp.(MOS)[b] (ks)	Exp.(pn)[b] (ks)
#1	2000 Jun 25	M31 Core	0112570401	00:42:43.0	41:15:46.1	28.9	24.9
#2	2000 Dec 28	M31 Core	0112570601	00:42:43.0	41:15:46.1	12.1	9.4
#3	2001 Jan 11	M31 G1	0065770101	00:32:46.9	39:34:41.7	7.3	4.9
#4	2001 Jun 29	M31 Core	0109270101	00:42:43.0	41:15:46.1	29.0	24.9
#5	2002 Jan 05	M31 North1	0109270701	00:44:01.0	41:35:57.0	57.3	54.7
#6	2002 Jan 06	M31 Core	0112570101	00:42:43.0	41:15:46.1	63.0	49.9
#7	2002 Jan 13	M31 South1	0112570201	00:41:25.0	40:55:35.0	53.9	53.3
#8	2002 Jan 24	M31 South2	0112570301	00:40:06.0	40:35:24.0	30.0	29.0
#9	2002 Jan 26	M31 North2	0109270301	00:45:20.0	41:56:09.0	29.1	25.3
#10	2002 Jun 29	M31 North3	0109270401	00:46:38.0	42:16:20.0	51.5	36.5

[a] – coordinates of the center of the field of view

[b] – instrument exposure used in the analysis

TABLE 2
Chandra OBSERVATIONS OF M31 FIELDS USED IN OUR ANALYSIS.

Obs. #	Date,UT (yyyy-mo-dd)	Field	Obs. ID/Instrument	R.A. (J2000)[a] (h:m:s)	Decl. (J2000)[a] (d:m:s)	Exp.[b] (ks)
	1999-10-13	M31 NUCLEUS	303/ACIS-I	00:42:42.59	41:16:12.2	12.0
	1999-12-11	M31 TRANSIENT	305/ACIS-I	00:42:44.40	41:16:08.3	4.1
	1999-12-23	M31 CENTER	268/HRC-I	00:42:44.40	41:16:08.3	5.2
	1999-12-27	M31 TRANSIENT	306/ACIS-I	00:42:44.40	41:16:08.3	4.1
	2000-01-29	M31 TRANSIENT	307/ACIS-I	00:42:44.40	41:16:08.3	4.1
	2000-02-16	M31 TRANSIENT	308/ACIS-I	00:42:44.40	41:16:08.3	4.0
	2000-03-08	M31 CENTER	271/HRC-I	00 42 44.40	41 16 08.3	2.4
	2000-06-01	M31 TRANSIENT	309/ACIS-S	00:42:44.40	41:16:08.3	5.1
	2000-07-02	M31 TRANSIENT	310/ACIS-S	00:42:44.40	41:16:08.3	5.1
	2000-07-29	M31 TRANSIENT	311/ACIS-I	00:42:44.40	41:16:08.3	4.9
	2000-08-27	M31 TRANSIENT	312/ACIS-I	00:42:44.40	41:16:08.3	4.7
	2000-09-21	M31 TRANSIENT	313/ACIS-S	00:42:40.80	40:51:54.0	6.1
	2000-10-21	M31 TRANSIENT	314/ACIS-S	00:42:40.80	40:51:54.0	5.1
	2000-11-01	M31-3	2052/ACIS-S	00:46:16.70	41:40:55.0	14.1
	2000-11-05	M31-2	2049/ACIS-S	00:41:49.90	40:59:20.0	14.8
	2000-11-17	M31 TRANSIENT	1580/ACIS-S	00:42:40.80	40:51:54.0	5.1
	2000-12-13	M31 NUCLEUS	1581/ACIS-I	00:42:44.40	41:16:08.3	4.4
	2001-01-13	M31 TRANSIENT	1854/ACIS-S	00:42:40.80	41:15:54.0	4.7
	2001-02-18	M31 NUCLEUS	1582/ACIS-I	00:42:44.40	41:16:08.3	4.3
	2001-03-08	M31-3	2053/ACIS-S	00:46:16.70	41:40:55.0	13.5
	2001-03-08	M31-2	2050/ACIS-S	00:41:49.90	40:59:20.0	13.2
	2001-06-10	M31 NUCLEUS	1583/ACIS-I	00:42:44.40	41:16:08.3	5.0
	2001-07-03	M31 NUCLEUS	1584/ACIS-I	00:42:37.50	40:54:27.0	4.9
	2001-07-03	M31-3	2054/ACIS-S	00:46:16.70	41:40:55.0	14.7
	2001-07-03	M31-2	2051/ACIS-S	00:41:49.90	40:59:20.0	13.8
	2001-07-24	M32	2017/ACIS-S	00:42:41.80	40:51:52.0	46.4
	2001-07-28	M32	2494/ACIS-S	00:42:41.80	40:51:52.0	16.1
	2001-08-31	M31 NUCLEUS	1577/ACIS-I	00:43:08.50	41:18:20.0	4.9
	2001-10-05	M31 NUCLEUS	1575/ACIS-S	00:42:44.40	41:16:08.3	38.1
	2001-10-05	M31 NUCLEUS	1576/ACIS-I	00:42:34.89	40:57:21.0	4.9
	2001-10-31	M31	1912/HRC-I	00:42:42.30	41:16:08.4	46.9
	2001-11-19	M31 NUCLEUS	1585/ACIS-I	00:43:05.55	41:17:03.3	4.9
	2001-12-07	M31 TRANSIENT	2895/ACIS-I	00:43:08.50	41:18:20.0	4.9
	2002-01-08	M31 TRANSIENT	2897/ACIS-I	00:43:09.80	41:19:00.7	4.9
	2002-02-06	M31 TRANSIENT	2896/ACIS-I	00:43:05.50	41:17:03.3	4.9
	2002-06-02	M31 TRANSIENT	2898/ACIS-I	00:43:09.80	41:19:00.7	4.9
	2002-07-08	M31 TRANSIENT	2901/ACIS-I	00:41:54.67	40:56:47.5	4.6
	2002-08-11	M31	4360/ACIS-I	00:42:44.40	41:16:08.9	4.9
	2002-08-23	M31 TRANSIENT	2899/ACIS-I	00:41:54.69	40:56:47.8	4.9
	2002-10-14	M31 TRANSIENT	2894/ACIS-I	00:42:34.90	40:57:21.0	4.7

[a] – coordinates of the center of the field of view

[b] – total exposure

TABLE 3
LIST OF GC X-RAY SOURCES DETECTED IN *XMM-Newton* AND *Chandra* OBSERVATIONS OF M31.

Source ID	R.A.	Decl.	L_X(0.3-10 keV) ($\times 10^{35}$ ergs s^{-1})	Optical ID[a]	X-ray ID[b]
1	00 32 46.6	39 34 40	6	G1	
2	00 40 20.3	40 43 57	1990	Bo5	SHP73
3	00 41 41.0	41 04 01	3	MIT87	D27
4	00 41 50.5	41 12 12	2.4-2.9	Bo55	
5	00 41 52.9	40 47 10	1-24	Bo58,MIT106	D22
6	00 42 06.1	41 02 48	31-73	Bo D42,MIT130	SHP138,D13
7	00 42 07.1	41 00 16	40-100	Bo D44	D15
8	00 42 09.5	41 17 45	40-114	MIT140	D10
9	00 42 12.1	41 17 58	24-300	Bo78,MIT153	D20
10	00 42 15.8	41 01 14	1735-2330	Bo82,MIT159	SHP150,D2
11	00 42 18.6	41 14 01	498-763	Bo86,MIT164	SHP158,D4
12	00 42 19.6	41 21 53	5	MIT165/MIT166	D24
13	00 42 25.0	40 57 19	19	Bo94,MIT173	SHP168,D21
14	00 42 26.1	41 19 15	28-174	Bo96,MIT174	D14
15	00 42 27.4	40 59 36	1-12	Bo98	D25
16	00 42 31.2	41 19 38	56-290	Bo107,MIT192	SHP175,D16
17	00 42 33.1	41 03 28	41-52	Bo110	SHP178
18	00 42 34.4	40 57 09	14	Bo117	
19	00 42 40.6	41 10 32	16-27	Bo123,MIT212	D18
20	00 42 41.4	41 15 23	34-137	MIT213	D23
21	00 42 50.7	41 10 33	3	MIT222	D28
22	00 42 51.9	41 31 07	3093-4009	Bo135	SHP205
23	00 42 55.5	41 18 35	8-84	Bo138	
24	00 42 59.6	41 19 19	152-555	Bo143	SHP217,D5
25	00 42 59.8	41 16 05	216-512	Bo144	D6
26	00 43 01.3	41 30 17	553-692	Bo91,MIT236	SHP218
27	00 43 02.9	41 15 22	74-414	Bo146	SHP220,D7
28	00 43 03.3	41 21 22	52-194	Bo147,MIT240	SHP222,D11
29	00 43 03.8	41 18 05	105-418	Bo148	SHP223,D8
30	00 43 07.5	41 20 20	16-72	Bo150,MIT246	D19
31	00 43 10.6	41 14 50	373-1248	Bo153,MIT251	SHP228,D3
32	00 43 14.2	41 07 24	600-1880	Bo158	SHP229,D12
33	00 43 14.7	41 25 13	2	Bo159	
34	00 43 15.4	41 11 24	16-22	Bo161,MIT260	D26
35	00 43 17.8	41 27 45	$< 1 - 1010$	Bo163	RX J0043.2+4127
36	00 43 36.7	41 08 10	46	Bo182	
37	00 43 37.3	41 14 43	454-1981	Bo185,MIT299	SHP247,D9
38	00 43 42.9	41 28 50	52	MIT311	SHP250
39	00 43 45.5	41 36 57	44	Bo193	SHP253
40	00 43 56.5	41 22 02	37	Bo204	SHP261
41	00 44 29.6	41 21 36	1130	Bo225	SHP282
42	00 45 45.4	41 39 42	5148-10372	Bo375	SHP318,D1
43	00 46 27.0	42 01 51	1496	Bo386	SHP349

[a] – source identifications beginning with Bo refer to Globular Cluster candidates listed in Table IV of Battistini et al. (1987), MIT – in Magnier (1993).

[b] – source identifications beginning with SHP refer to M31 *ROSAT*/PSPC X-ray source catalog entries from Supper et al. (1997, 2001). Identifications beginning with D refer to the list of GC X-ray sources listed in Table 3 of DiStefano et al. (2002).

TABLE 4

BEST-FIT MODEL PARAMETERS OF THE ENERGY SPECTRA OF THE BRIGHT GC SOURCES. *XMM-Newton*/EPIC DATA, $0.3-10$ KEV ENERGY RANGE. ABSORBED SIMPLE POWER LAW MODEL APPROXIMATION. PARAMETER ERRORS CORRESPOND TO THE 1σ LEVEL.

ID [a]						Observation/Instrument
	Model: Absorbed Power Law (POWERLAW*WABS)					
	Photon Index	N_H [b]	Flux [c]	χ^2 (dof)	L_X [d]	
2	1.55 ± 0.03	0.15 ± 0.01	28.80 ± 0.32	186.3(181)	1990	xmm 8/(MOS1+MOS2)
6	$1.84^{+0.17}_{-0.10}$	< 0.05	0.81 ± 0.06	32.1(29)	56	xmm 7/(MOS1+MOS2)
7	$1.70^{+0.19}_{-0.16}$	$0.31^{+0.09}_{-0.06}$	1.44 ± 0.07	50.4(49)	99	xmm 7/(MOS1+MOS2)
8	$2.18^{+0.13}_{-0.15}$	$0.33^{+0.03}_{-0.05}$	0.93 ± 0.07	30.2(29)	64	xmm 1/pn
	$2.33^{+0.25}_{-0.18}$	$0.45^{+0.08}_{-0.07}$	0.80 ± 0.06	23.8(30)	55	xmm 4/pn
	$2.13^{+0.08}_{-0.11}$	$0.37^{+0.02}_{-0.04}$	1.65 ± 0.07	72.6(73)	114	xmm 6/pn
9	$2.53^{+0.21}_{-0.28}$	$0.61^{+0.20}_{-0.11}$	0.58 ± 0.06	18.2(15)	40	xmm 1/pn
	$2.44^{+0.20}_{-0.26}$	0.54 ± 0.10	0.74 ± 0.06	29.7(33)	51	xmm 4/pn
	$1.83^{+0.08}_{-0.06}$	$0.51^{+0.06}_{-0.04}$	3.25 ± 0.10	83.5(105)	225	xmm 6/pn
10	$1.37^{+0.05}_{-0.07}$	0.44 ± 0.03	32.20 ± 0.64	94.6(94)	2226	xmm 4/pn
	1.52 ± 0.03	$0.49^{+0.01}_{-0.02}$	31.40 ± 0.30	231.2(293)	2170	xmm 7/(MOS1+MOS2+pn)
11	$1.42^{+0.04}_{-0.07}$	0.09 ± 0.02	9.72 ± 0.20	115.2(113)	672	xmm 1/(MOS1+MOS2)
	1.34 ± 0.06	0.09 ± 0.02	9.45 ± 0.29	72.5(60)	653	xmm 2/pn
	1.61 ± 0.04	$0.14^{+0.01}_{-0.04}$	8.29 ± 0.25	195.9(189)	573	xmm 4/(MOS1+pn)
	1.56 ± 0.03	0.12 ± 0.01	8.27 ± 0.09	563.1(508)	571	xmm 6/(MOS1+MOS2+pn)
14	$1.90^{+0.07}_{-0.06}$	$0.25^{+0.05}_{-0.01}$	1.87 ± 0.06	125.7(97)	129	xmm 1/(MOS1+MOS2+pn)
	1.81 ± 0.06	$0.31^{+0.03}_{-0.02}$	2.20 ± 0.06	157.7(145)	152	xmm 4/(MOS1+MOS2+pn)
	$2.30^{+0.05}_{-0.06}$	$0.31^{+0.04}_{-0.02}$	0.98 ± 0.04	127.2(138)	68	xmm 6/(MOS1+MOS2+pn)
16	$1.84^{+0.08}_{-0.07}$	$0.15^{+0.02}_{-0.03}$	1.18 ± 0.05	93.0(89)	82	xmm 1/(MOS1+MOS2+pn)
	$1.78^{+0.19}_{-0.08}$	$0.20^{+0.07}_{-0.05}$	2.73 ± 0.20	34.6(26)	190	xmm 2/pn
	$1.91^{+0.04}_{-0.05}$	$0.22^{+0.01}_{-0.03}$	3.36 ± 0.07	184.5(209)	232	xmm 4/(MOS1+MOS2+pn)
	$2.17^{+0.04}_{-0.03}$	$0.27^{+0.01}_{-0.04}$	2.12 ± 0.04	208.8(243)	147	xmm 6/(MOS1+MOS2+pn)
19	$1.52^{+0.34}_{-0.19}$	< 0.06	3.10 ± 0.28	70.8(62)	21	xmm 4/pn+xmm 6/pn
20	$1.82^{+0.07}_{-0.08}$	0.12 ± 0.02	1.99 ± 0.08	238.1(214)	137	xmm 6/pn
22	$1.57^{+0.03}_{-0.02}$	0.26 ± 0.01	52.95 ± 0.42	443.7(424)	3651	xmm 5/(MOS1+MOS2)
24	$1.92^{+0.03}_{-0.04}$	0.13 ± 0.01	4.39 ± 0.09	213.4(199)	304	xmm 1/(MOS1+MOS2+pn)
	2.11 ± 0.11	$0.18^{+0.02}_{-0.05}$	4.69 ± 0.19	51.0(63)	324	xmm 2/pn
	$1.94^{+0.05}_{-0.04}$	0.14 ± 0.01	5.21 ± 0.09	304.0(284)	360	xmm 4/(MOS1+MOS2+pn)
	1.92 ± 0.02	0.12 ± 0.01	5.68 ± 0.08	486.3(450)	393	xmm 6/(MOS1+MOS2+pn)
25	1.60 ± 0.04	0.13 ± 0.01	5.31 ± 0.10	197.7(201)	367	xmm 1/(MOS1+MOS2+pn)
	$1.48^{+0.03}_{-0.01}$	$0.09^{+0.02}_{-0.01}$	7.64 ± 0.11	320.6(316)	528	xmm 4/(MOS1+MOS2+pn)
	$1.57^{+0.02}_{-0.03}$	0.13 ± 0.01	7.15 ± 0.09	524.7(517)	495	xmm 6/(MOS1+MOS2+pn)
26	$0.83^{+0.04}_{-0.03}$	$0.07^{+0.01}_{-0.02}$	8.91 ± 0.20	228.0(176)	614	xmm 5/(MOS1+MOS2) +xmm 6/pn
28	$2.23^{+0.05}_{-0.07}$	0.12 ± 0.02	1.94 ± 0.05	81.7(91)	134	xmm 1/(MOS1+MOS2+pn)
	$2.25^{+0.05}_{-0.06}$	0.12 ± 0.02	1.87 ± 0.05	132.7(118)	129	xmm 4/(MOS2+pn)
	2.13 ± 0.06	$0.11^{+0.02}_{-0.01}$	1.62 ± 0.04	84.8(87)	112	xmm 6/pn
29	2.12 ± 0.04	$0.14^{+0.02}_{-0.01}$	2.80 ± 0.07	145.4(164)	194	xmm 1/(MOS1+MOS2+pn)
	$1.82^{+0.08}_{-0.07}$	$0.10^{+0.03}_{-0.01}$	4.52 ± 0.20	36.0(46)	313	xmm 2/pn
	$1.61^{+0.03}_{-0.02}$	0.09 ± 0.01	6.50 ± 0.11	320.4(333)	450	xmm 4/(MOS1+MOS2+pn)
	1.96 ± 0.04	$0.16^{+0.01}_{-0.02}$	4.19 ± 0.09	315.0(282)	290	xmm 6/(MOS1+MOS2+pn)
30	$2.87^{+0.45}_{-0.28}$	$0.15^{+0.07}_{-0.04}$	0.35 ± 0.03	34.9(36)	25	xmm 4/pn
31	1.56 ± 0.02	0.09 ± 0.01	15.95 ± 0.18	483.4(463)	1103	xmm 1/(MOS1+MOS2+pn)
	$1.68^{+0.04}_{-0.03}$	0.10 ± 0.01	16.56 ± 0.38	163.0(202)	1144	xmm 2/(MOS1+MOS2+pn)
	$1.71^{+0.01}_{-0.03}$	0.10 ± 0.01	13.31 ± 0.18	554.7(571)	920	xmm 4/(MOS1+MOS2+pn)
	1.66 ± 0.02	0.09 ± 0.01	12.53 ± 0.16	731.6(759)	866	xmm 6/(MOS1+MOS2+pn)
32	0.67 ± 0.04	0.12 ± 0.03	18.64 ± 0.38	207.0(182)	1288	xmm 1/(MOS1+MOS2+pn)
	$0.74^{+0.06}_{-0.05}$	$0.04^{+0.03}_{-0.01}$	20.03 ± 0.66	90.6(48)	1384	xmm 2/pn
	0.56 ± 0.02	< 0.05	26.07 ± 0.34	412.4(348)	1802	xmm 4/(MOS1+MOS2+pn)
	0.57 ± 0.03	0.04 ± 0.02	10.82 ± 0.19	326.0(249)	748	xmm 6/(MOS1+MOS2+pn)
34	$2.08^{+0.32}_{-0.43}$	$0.10^{+0.05}_{-0.04}$	0.27 ± 0.02	53.1(62)	19	xmm 1/pn+xmm 6/pn
36	$1.36^{+0.39}_{-0.26}$	$0.23^{+0.23}_{-0.11}$	0.66 ± 0.07	20.7(33)	46	xmm 6/pn
37	$1.41^{+0.01}_{-0.05}$	0.07 ± 0.01	10.87 ± 0.17	181.8(200)	751	xmm 1/(MOS1+MOS2+pn)
	$1.55^{+0.10}_{-0.09}$	0.08 ± 0.02	8.77 ± 0.34	33.8(39)	606	xmm 2/pn
	$1.44^{+0.03}_{-0.02}$	0.09 ± 0.01	10.85 ± 0.15	317.1(282)	750	xmm 4/(MOS1+MOS2+pn)
	1.68 ± 0.03	$0.12^{+0.01}_{-0.02}$	9.24 ± 0.10	401.7(352)	640	xmm 6/(MOS1+MOS2+pn)
38	$1.61^{+0.14}_{-0.13}$	0.23 ± 0.05	0.75 ± 0.05	33.2(32)	52	xmm 5/pn
39	$1.61^{+0.11}_{-0.04}$	0.04 ± 0.03	0.64 ± 0.03	26.3(26)	44	xmm 5/(MOS1+MOS2)
40	1.90 ± 0.32	0.19 ± 0.07	0.54 ± 0.05	14.6(16)	37	xmm 6/pn
43	1.56 ± 0.04	0.13 ± 0.01	21.80 ± 0.30	238.3(199)	1507	xmm 9/(MOS1+MOS2+pn)

[a] – Source number in Table 3

[b] – Equivalent hydrogen column depth in units of 10^{22} cm^{-2}

[c] – Absorbed model flux in the $0.3-10$ keV energy range in units of 10^{-13} erg s^{-1} cm^{-2}

[d] – Absorbed isotropic source luminosity in the $0.3-10.0$ keV energy range in units of 10^{35} erg s^{-1} assuming the distance of 760 kpc

TABLE 5

BEST-FIT MODEL PARAMETERS OF THE ENERGY SPECTRA OF THE BRIGHT GC SOURCES. *Chandra*/ACIS DATA, $0.5-7.0$ KEV ENERGY RANGE. ABSORBED SIMPLE POWER LAW MODEL APPROXIMATION. PARAMETER ERRORS CORRESPOND TO THE 1σ LEVEL.

ID [a]						Observation/Instrument
	Model: Absorbed Power Law (POWERLAW*WABS)					
	Photon Index	N_H^b	Flux[c]	χ^2 (dof)	L_X^d	
6	$2.04^{+0.31}_{-0.17}$	< 0.08	0.49 ± 0.04	16.8(17)	34	2017/ACIS
7	$1.93^{+0.44}_{-0.25}$	$0.60^{+0.33}_{-0.20}$	0.73 ± 0.06	31.2(23)	51	2017/ACIS
8	$2.29^{+0.19}_{-0.16}$	$0.35^{+0.06}_{-0.05}$	1.15 ± 0.06	21.3(26)	80	1575/ACIS
9	$2.07^{+0.08}_{-0.09}$	$0.51^{+0.08}_{-0.06}$	2.07 ± 0.08	20.9(39)	143	1575/ACIS
10	1.47 ± 0.15	0.56 ± 0.14	25.35 ± 1.00	27.4(28)	1752	1580/ACIS
	$1.48^{+0.15}_{-0.14}$	$0.64^{+0.10}_{-0.14}$	28.48 ± 1.07	27.6(25)	1968	1584/ACIS
	$1.46^{+0.03}_{-0.04}$	0.49 ± 0.03	33.72 ± 0.40	238.6(176)	2330	2017/ACIS
	$1.49^{+0.11}_{-0.13}$	$0.54^{+0.13}_{-0.11}$	28.57 ± 1.05	31.8(32)	1975	2901/ACIS
11	1.44 ± 0.06	0.14 ± 0.03	7.87 ± 0.18	86.4(65)	544	1575/ACIS
14	$2.40^{+0.30}_{-0.19}$	$0.31^{+0.09}_{-0.04}$	0.91 ± 0.05	19.6(15)	63	1575/ACIS
16	$1.73^{+0.11}_{-0.09}$	$0.24^{+0.04}_{-0.03}$	3.94 ± 0.14	37.2(34)	272	1575/ACIS
20	$1.90^{+0.17}_{-0.30}$	$0.20^{-0.12}_{+0.03}$	0.50 ± 0.04	10.8(10)	35	1575/ACIS
22	1.48 ± 0.08	$0.22^{+0.03}_{-0.02}$	49.48 ± 1.23	60.8(62)	3420	309/ACIS
	$1.66^{+0.12}_{-0.11}$	$0.35^{+0.06}_{-0.10}$	47.61 ± 1.46	34.8(38)	3290	1582/ACIS
	1.51 ± 0.03	0.30 ± 0.02	59.80 ± 0.56	261.7(215)	4130	1575/ACIS
23	$1.71^{+0.17}_{-0.12}$	< 0.06	0.54 ± 0.04	14.6(19)	38	1575/ACIS
24	1.84 ± 0.05	$0.15^{+0.02}_{-0.01}$	6.02 ± 0.12	90.3(84)	416	1575/ACIS
25	1.36 ± 0.05	0.07 ± 0.01	7.87 ± 0.15	78.8(84)	544	1575/ACIS
26	$0.91^{+0.07}_{-0.06}$	$0.04^{+0.04}_{-0.03}$	8.37 ± 0.25	76.4(61)	578	1575/ACIS
27	$2.02^{+0.07}_{-0.06}$	0.04 ± 0.02	1.42 ± 0.05	33.0(25)	98	1575/ACIS
29	$1.84^{+0.25}_{-0.10}$	$0.17^{+0.10}_{-0.07}$	2.64 ± 0.16	20.4(25)	183	303/ACIS
	1.96 ± 0.07	$0.13^{+0.02}_{-0.01}$	3.65 ± 0.09	76.6(56)	252	1575/ACIS
30	$1.69^{+0.24}_{-0.27}$	$0.26^{+0.18}_{-0.09}$	0.43 ± 0.04	12.6(16)	30	1575/ACIS
31	$1.41^{+0.08}_{-0.04}$	0.11 ± 0.03	15.88 ± 0.44	54.7(59)	1097	303/ACIS
	1.52 ± 0.04	0.06 ± 0.01	14.21 ± 0.20	210.4(171)	982	1575/ACIS
32	$0.60^{+0.10}_{-0.11}$	< 0.08	16.27 ± 0.99	18.3(20)	1125	310/ACIS
	0.26 ± 0.14	$0.03^{+0.11}_{-0.03}$	27.23 ± 1.52	10.3(19)	1880	1854/ACIS
	$0.59^{+0.11}_{-0.09}$	$0.26^{+0.04}_{-0.16}$	8.68 ± 0.34	82.1(85)	600	2017/ACIS
	$0.50^{+0.14}_{-0.11}$	$0.18^{+0.13}_{-0.11}$	14.12 ± 0.67	47.2(33)	976	2494/ACIS
35	$1.54^{+0.14}_{-0.13}$	0.11 ± 0.04	15.30 ± 0.71	30.9(23)	1057	1582/ACIS
37	1.40 ± 0.04	< 0.04	10.32 ± 0.23	102.8(93)	713	1575/ACIS
41	$1.44^{+0.15}_{-0.10}$	< 0.09	16.02 ± 0.69	29.3(28)	1107	2895/ACIS
	$1.55^{+0.19}_{-0.14}$	$0.04^{+0.06}_{-0.01}$	16.84 ± 0.88	10.9(17)	1164	2896/ACIS
	$1.58^{+0.16}_{-0.15}$	$0.08^{+0.07}_{-0.05}$	16.35 ± 0.77	22.2(22)	1130	2897/ACIS
42	1.66 ± 0.06	0.28 ± 0.03	74.50 ± 1.43	134.2(108)	5148	2052/ACIS
	$1.75^{+0.07}_{-0.06}$	$0.28^{+0.03}_{-0.02}$	150.0 ± 3.0	102.9(69)	10372	2053/ACIS

[a] – Source number in Table 3

[b] – Equivalent hydrogen column depth in units of 10^{22} cm^{-2}

[c] – Absorbed model flux in the $0.3-10$ keV energy range in units of 10^{-13} erg s^{-1} cm^{-2}

[d] – Absorbed isotropic source luminosity in the $0.3-10.0$ keV energy range in units of 10^{35} erg s^{-1} assuming the distance of 760 kpc

TABLE 6

BRIGHT GCS SPECTRAL FIT RESULTS (*XMM-Newton*/EPIC DATA, $0.3-10$ KEV ENERGY RANGE; *Chandra*/ACIS DATA, $0.5-7.0$ KEV ENERGY RANGE). ABSORBED CUT-OFF POWER LAW AND COMPTONIZATION MODELS. PARAMETER ERRORS CORRESPOND TO 1σ LEVEL.

ID [a]								Remarks
Model: Absorbed Cutoff Power Law (CUTOFFPL*WABS)								
	Photon Index	Cutoff Energy (keV)		$N_{\rm H}^{b}$	Flux[c]	χ^2 (dof)	L_X^d	
22	$0.64^{+0.13}_{-0.16}$	$3.64^{+0.80}_{-0.55}$		$0.16^{+0.03}_{-0.02}$	53.07 ± 0.52	228.2(215)	3668	*chandra 1575*
	$0.83^{+0.13}_{-0.10}$	$4.13^{+0.84}_{-0.50}$		$0.16^{+0.02}_{-0.01}$	47.74 ± 0.40	399.3(423)	3300	*xmm 5*
26	0.18 ± 0.09	$4.86^{+1.12}_{-0.72}$		< 0.02	7.91 ± 0.17	208.0(175)	545	*xmm 5+xmm 6*
32	-0.15 ± 0.09	$4.40^{+0.46}_{-0.53}$		< 0.03	16.71 ± 0.28	171.8(181)	1155	*xmm 1*
	0.17 ± 0.15	$5.43^{+2.05}_{-1.20}$		< 0.02	18.59 ± 0.61	77.4(47)	1285	*xmm 2*
	0.21 ± 0.07	$7.91^{+1.75}_{-1.15}$		< 0.01	23.71 ± 0.31	376.6(347)	1640	*xmm 4*
	$0.01^{+0.05}_{-0.08}$	$5.74^{+0.65}_{-1.05}$		< 0.01	10.69 ± 0.17	278.0(248)	739	*xmm 6*
42	$0.83^{+0.32}_{-0.24}$	$3.83^{+2.35}_{-0.97}$		0.16 ± 0.05	68.39 ± 1.32	126.4(107)	4726	*chandra 2052*
	$0.13^{+0.31}_{-0.32}$	$1.81^{+0.45}_{-0.31}$		0.09 ± 0.03	125.9 ± 2.6	74.2(68)	8700	*chandra 2053*
43	$1.13^{+0.17}_{-0.24}$	$6.82^{+4.47}_{-1.94}$		0.09 ± 0.02	20.39 ± 0.29	232.0(198)	1409	*xmm 9*
Model: Absorbed Comptonization Model (COMPTT*WABS)								
	kT_0 (keV)	kT_e (keV)	τ	$N_{\rm H}^{b}$	Flux[c]	χ^2 (dof)	L_X^d	
22	$0.20^{+0.04}_{-0.15}$	$1.46^{+0.08}_{-0.07}$	$26.3^{+1.6}_{-2.0}$	$0.17^{+0.09}_{-0.07}$	50.29 ± 0.49	229.2(217)	3475	*chandra 1575*
	$0.37^{+0.01}_{-0.03}$	$1.88^{+0.23}_{-0.18}$	$19.5^{+0.9}_{-1.6}$	< 0.09	47.82 ± 0.41	398.7(422)	3297	*xmm 5*
26	$0.03^{+0.07}_{-0.01}$	$1.76^{+0.14}_{-0.12}$	$34.6^{+2.8}_{-2.5}$	$0.07^{+0.01}_{-0.02}$	7.38 ± 0.16	206.8(174)	509	*xmm 5+xmm 6*
32	$0.06^{+0.05}_{-0.06}$	$1.87^{+0.12}_{-0.10}$	$38.6^{+2.9}_{-2.7}$	$0.10^{+0.03}_{-0.04}$	16.11 ± 0.27	177.0(180)	1113	*xmm 1*
	$0.07^{+0.06}_{-0.06}$	$1.63^{+0.13}_{-0.10}$	$44.8^{+3.8}_{-4.6}$	< 0.09	17.63 ± 0.58	65.5(46)	1220	*xmm 2*
	$0.09^{+0.02}_{-0.08}$	$1.82^{+0.08}_{-0.06}$	$43.2^{+1.3}_{-2.1}$	< 0.06	21.63 ± 0.28	341.7(346)	1495	*xmm 4*
	$0.10^{+0.05}_{-0.09}$	$1.79^{+0.08}_{-0.07}$	$45.2^{+3.7}_{-2.7}$	$0.03^{+0.03}_{-0.01}$	9.93 ± 0.16	252.3(247)	686	*xmm 6*
42	$0.17^{+0.05}_{-0.06}$	$1.45^{+0.25}_{-0.14}$	$23.7^{+2.9}_{-1.7}$	$0.19^{+0.03}_{-0.06}$	65.46 ± 1.26	125.7(106)	4524	*chandra 2052*
	< 0.14	$1.08^{+0.10}_{-0.08}$	$29.5^{+3.5}_{-3.0}$	0.18 ± 0.03	122.8 ± 2.5	71.2(67)	8485	*chandra 2053*
43	0.14 ± 0.04	$1.64^{+0.15}_{-0.16}$	$22.4^{+2.2}_{-2.3}$	0.09 ± 0.02	19.42 ± 0.28	258.3(235)	1339	*xmm 9*

[a] – Source number in Table 3

[b] – Equivalent hydrogen column depth in units of 10^{22} cm^{-2}

[c] – Absorbed model flux in the $0.3-10$ keV energy range in units of 10^{-13} erg s^{-1} cm^{-2}

[d] – Absorbed isotropic source luminosity in the $0.3-10.0$ keV energy range in units of 10^{35} erg s^{-1} assuming the distance of 760 kpc

TABLE 7

BRIGHT GCS SPECTRAL FIT RESULTS, *XMM-Newton*/EPIC AND *Chandra*/ACIS DATA. TWO-COMPONENT MODEL APPROXIMATION: (BBODYRAD+DISKBB)*WABS AND (BBODYRAD+POWERLAW)*WABS MODELS. PARAMETER ERRORS CORRESPOND TO 1σ LEVEL.

ID [a]								Observation
				Model: (BBODYRAD+DISKBB)*WABS				
	kT_{BB} (keV)	kT_{in} (keV)	$r_{in}\sqrt{cosi}$ (km)	$N_{\rm H}^{b}$	Flux[c]	χ^2 (dof)	L_X^d	
22	$1.40^{+0.25}_{-0.16}$	0.83 ± 0.16	37^{+13}_{-8}	0.17 ± 0.03	50.94 ± 0.50	229.3(217)	3520	*chandra 1575*
	$1.84^{+0.25}_{-0.27}$	$1.05^{+0.16}_{-0.14}$	26^{+5}_{-4}	0.14 ± 0.01	48.26 ± 0.42	395.1(421)	3335	*xmm 5*
42	...	1.70 ± 0.08	16^{+1}_{-2}	0.10 ± 0.02	65.31 ± 1.25	128.2(106)	4513	*chandra 2052*
	...	1.45 ± 0.07	30 ± 3	0.12 ± 0.02	125.4 ± 2.50	71.2(67)	8665	*chandra 2053*
43	$1.30^{+0.12}_{-0.11}$	0.55 ± 0.02	45^{+11}_{-8}	0.09 ± 0.02	19.48 ± 0.27	258.0(233)	1346	*xmm 9*
				Model: (BBODYRAD+POWERLAW)*WABS				
	kT_{BB} (keV)	Photon Index	r_{BB} (km)	$N_{\rm H}^{b}$	Flux[c]	χ^2 (dof)	L_X^d	
22	$1.10^{+0.09}_{-0.12}$	$1.82^{+0.28}_{-0.22}$	27 ± 3	0.28 ± 0.05	52.45 ± 0.52	229.0(217)	3625	*chandra 1575*
	$0.82^{+0.07}_{-0.05}$	$1.56^{+0.07}_{-0.06}$	28^{+6}_{-4}	$0.21^{+0.01}_{-0.02}$	49.87 ± 0.43	392.6(421)	3446	*xmm 5*
42	$0.87^{+0.26}_{-0.13}$	$1.67^{+0.44}_{-0.12}$	23^{+6}_{-8}	$0.22^{+0.06}_{-0.05}$	70.59 ± 1.35	125.2(106)	4878	*chandra 2052*
	$0.91^{+0.05}_{-0.04}$	$2.66^{+0.77}_{-0.43}$	82^{+12}_{-13}	$0.32^{+0.11}_{-0.06}$	122.9 ± 2.5	71.3(67)	8493	*chandra 2053*
43	$1.20^{+0.13}_{-0.12}$	$1.91^{+0.33}_{-0.19}$	16^{+2}_{-3}	$0.16^{+0.04}_{-0.02}$	20.20 ± 0.28	215.2(195)	1396	*xmm 9*

[a] – Source number in Table 3

[b] – Equivalent hydrogen column depth in units of 10^{22} cm^{-2}

[c] – Absorbed model flux in the $0.3-10$ keV energy range in units of 10^{-13} erg s^{-1} cm^{-2}

[d] – Absorbed isotropic source luminosity in the $0.3-10.0$ keV energy range in units of 10^{35} erg s^{-1} assuming the distance of 760 kpc

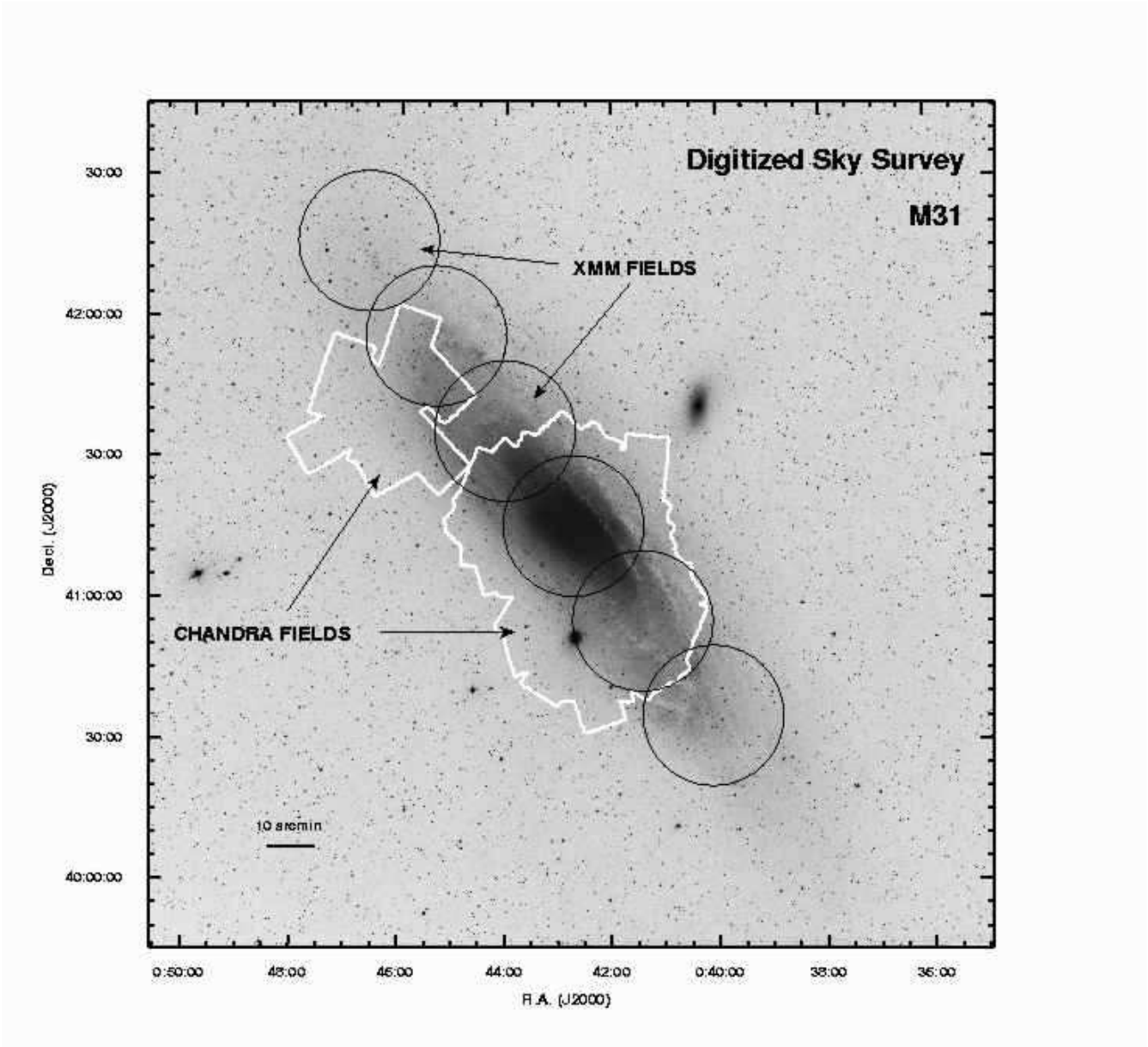

FIG. 1.— Optical image of M31 from the Digitized Sky Survey with regions covered by *XMM-Newton*/EPIC (*black circles*) and *Chandra*/ACIS/HRC observations (*white regions*). The remote globular cluster G1 field is located outside image boundary.

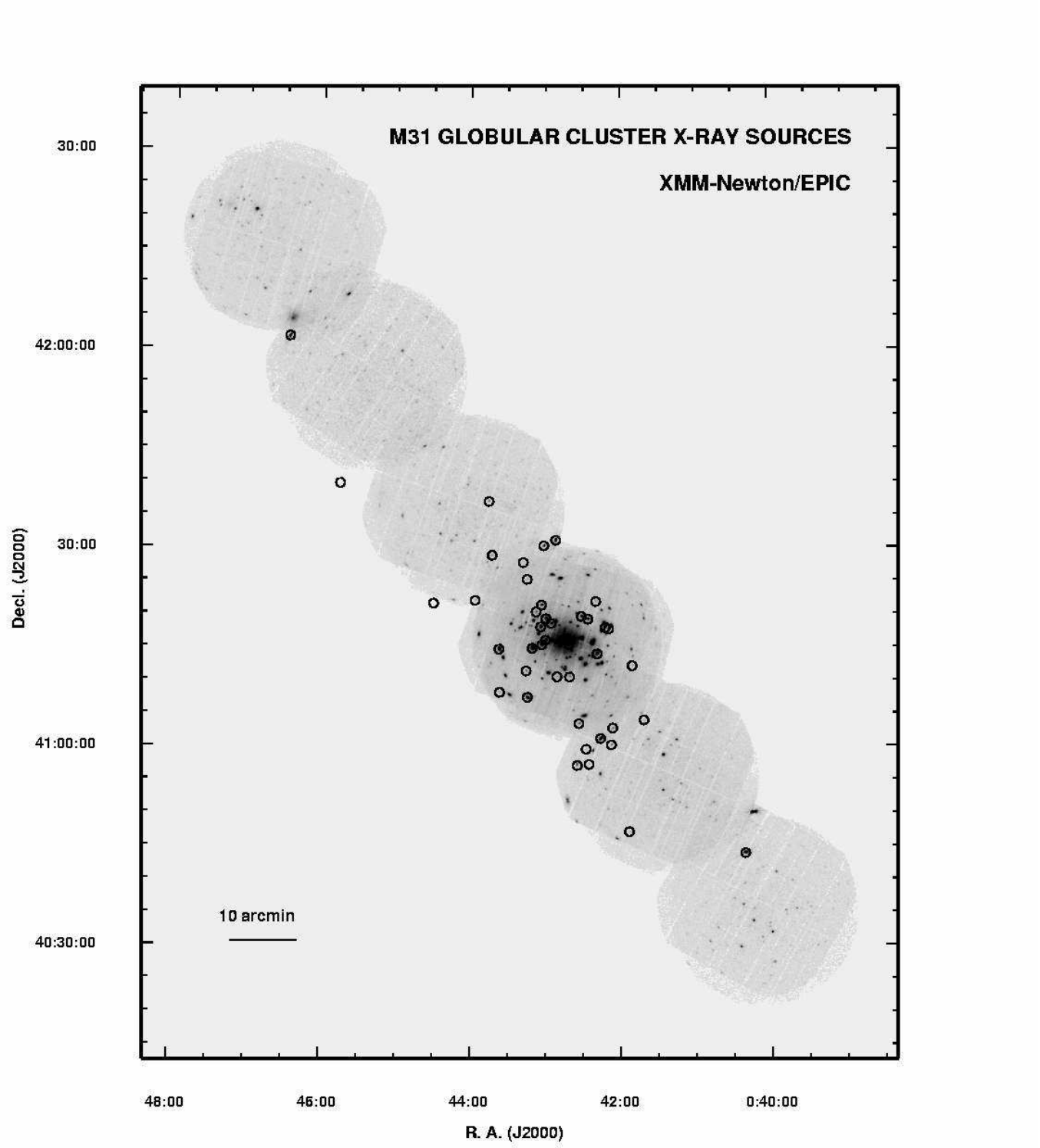

FIG. 2.— Combined *XMM*/EPIC images of M31 fields in the $0.3-7.0$ keV energy band. The image was convolved with circularly symmetric Gaussian function with $\sigma = 8''$. The globular cluster X-ray sources detected in *XMM-Newton* and *Chandra* observations are marked with circles.

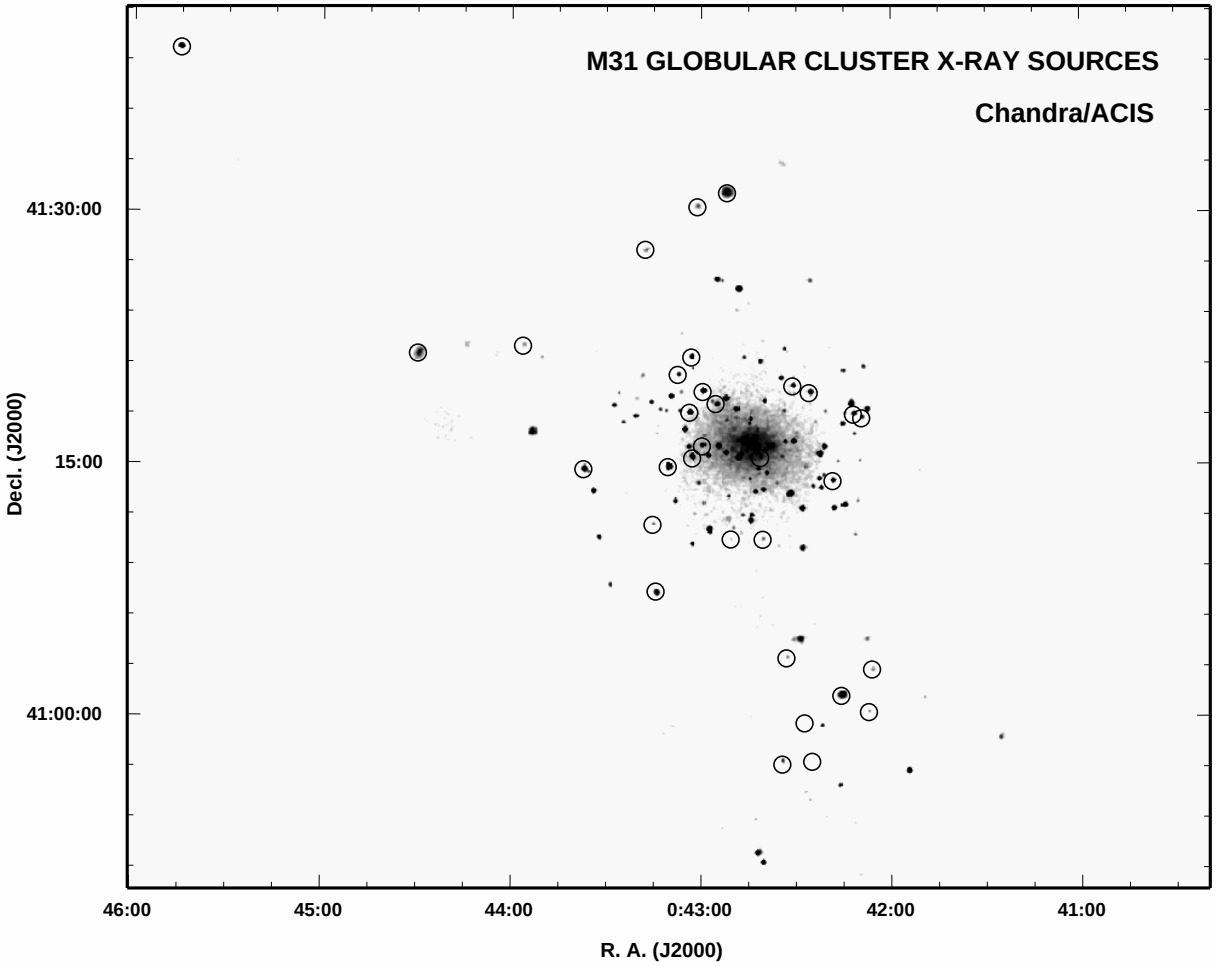

FIG. 3.— Combined *Chandra*/ACIS images of M31 fields in the $0.3 - 7.0$ keV energy band. The image was convolved with circularly symmetric Gaussian function with $\sigma = 8''$. The globular cluster X-ray sources detected with *Chandra* are marked with circles.

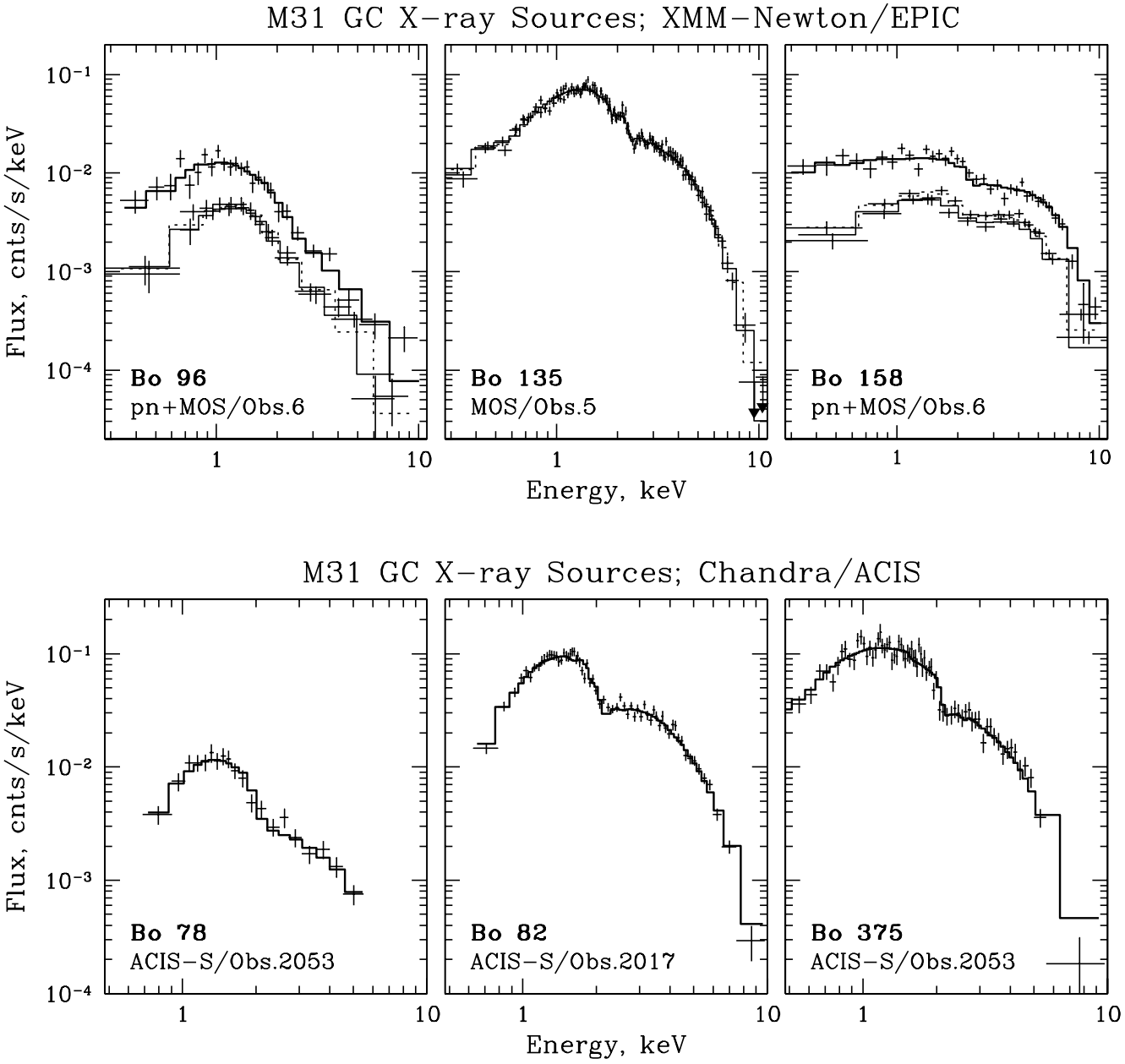

FIG. 4.— *Upper panels*: Representative *XMM-Newton*/EPIC spectra of the bright GC X-ray sources in the $0.3-10$ keV energy band. (EPIC-pn is always the upper spectrum and the two MOS spectra overlap). Corresponding model fits to the EPIC-pn, MOS1 and MOS2 spectra (Tables 4, 6, 7) are shown with thick, thin and dotted histograms respectively. *Left panel*: Bo 96 (#14), EPIC-pn and MOS1,2 data, fit by absorbed simple power law model. *Middle panel*: Bo 135 (#10), EPIC-MOS1 and MOS2 data, fit by absorbed power law model with exponential cutoff. *Right panel*: Bo 158 (#32), EPIC-pn and MOS1,2 data, fit by absorbed Comptonization model. *Lower panels*: *Chandra*/ACIS spectra of the bright GC X-ray sources. Model fits are shown with thick histograms (Tables 5, 6, 7). *Left panel*: Bo 78 (#9), ACIS-S data, $0.5-7$ keV energy range, fit by an absorbed simple power law model. *Middle panel*: Bo 82 (#10), ACIS-S data, $0.5-10$ keV energy range, fit by an absorbed simple power law model. *Right panel*: Bo 375 (#42), ACIS-S data, $0.5-10$ keV energy range, fit by an absorbed power law model with exponential cutoff.

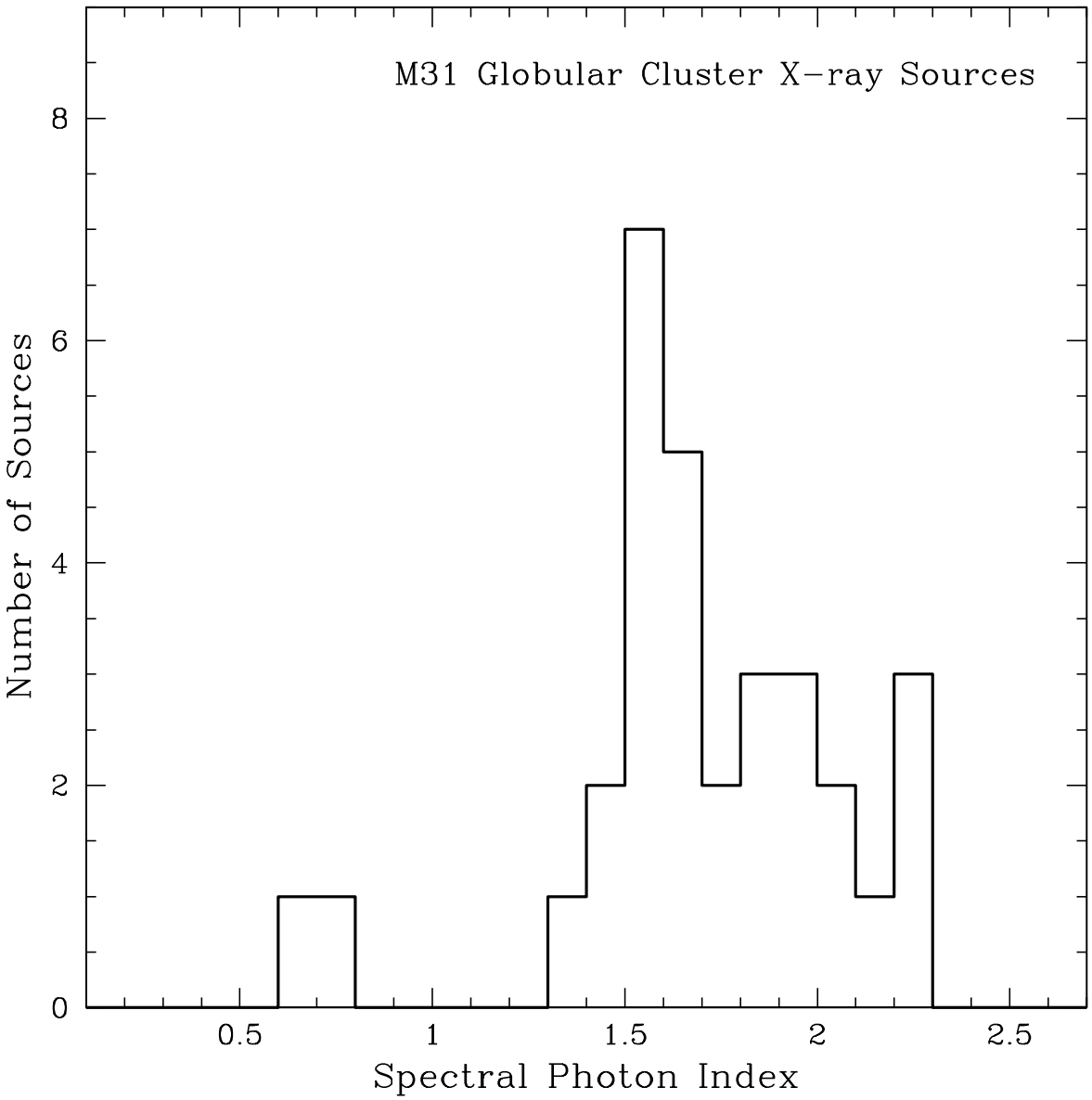

FIG. 5.— The distribution of the spectral slopes derived from the analysis of 31 bright GC X-ray sources. The histogram bins are 0.1 wide.

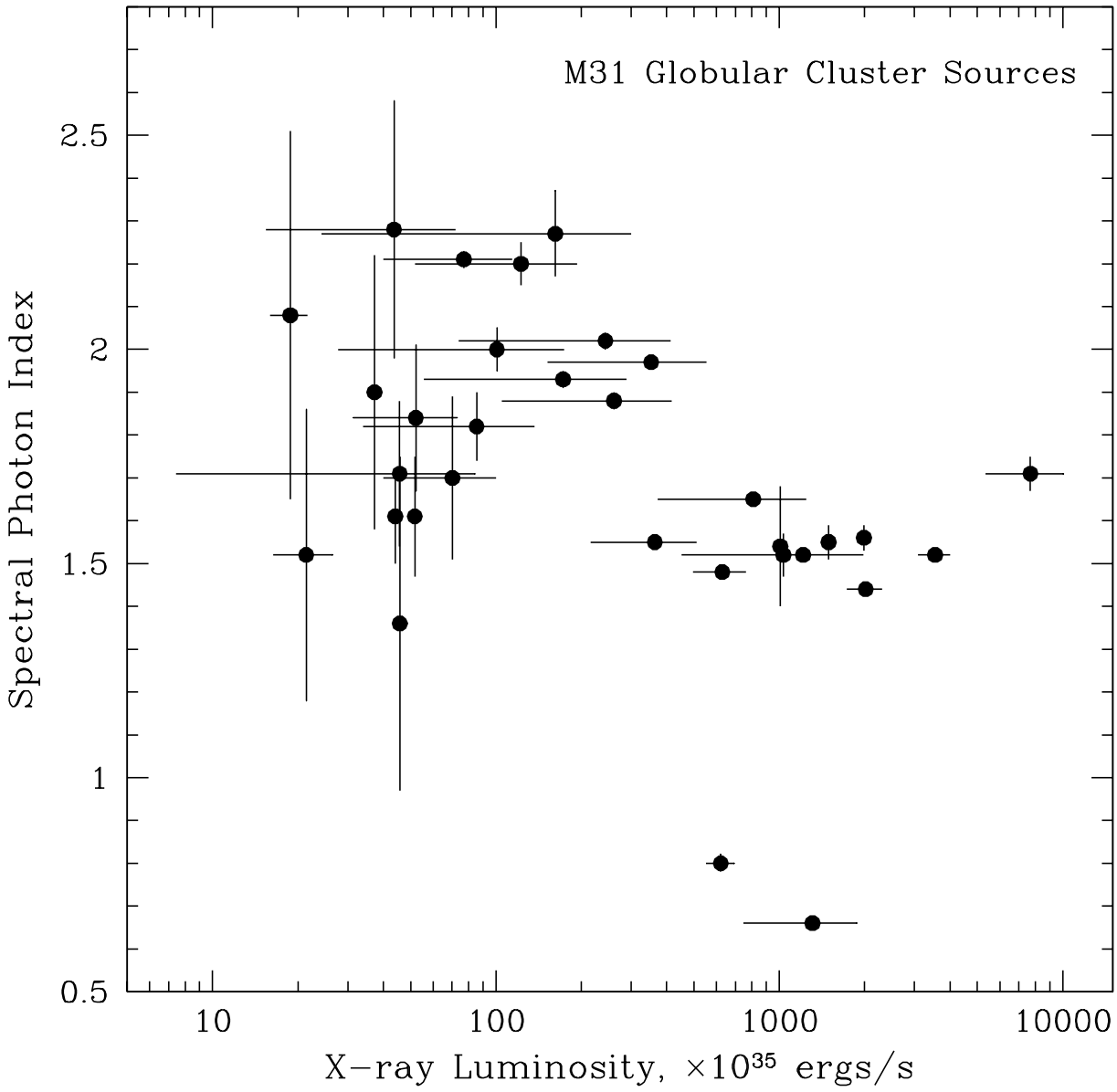

FIG. 6.— Spectral photon index of the GC X-ray sources in M31 vs. their X-ray luminosity in the $0.3-10$ keV energy band. The error bars in X-axis reflect statistical uncertainty of the source flux determination and in some cases the range of source X-ray luminosities observed with *XMM* and *Chandra*.

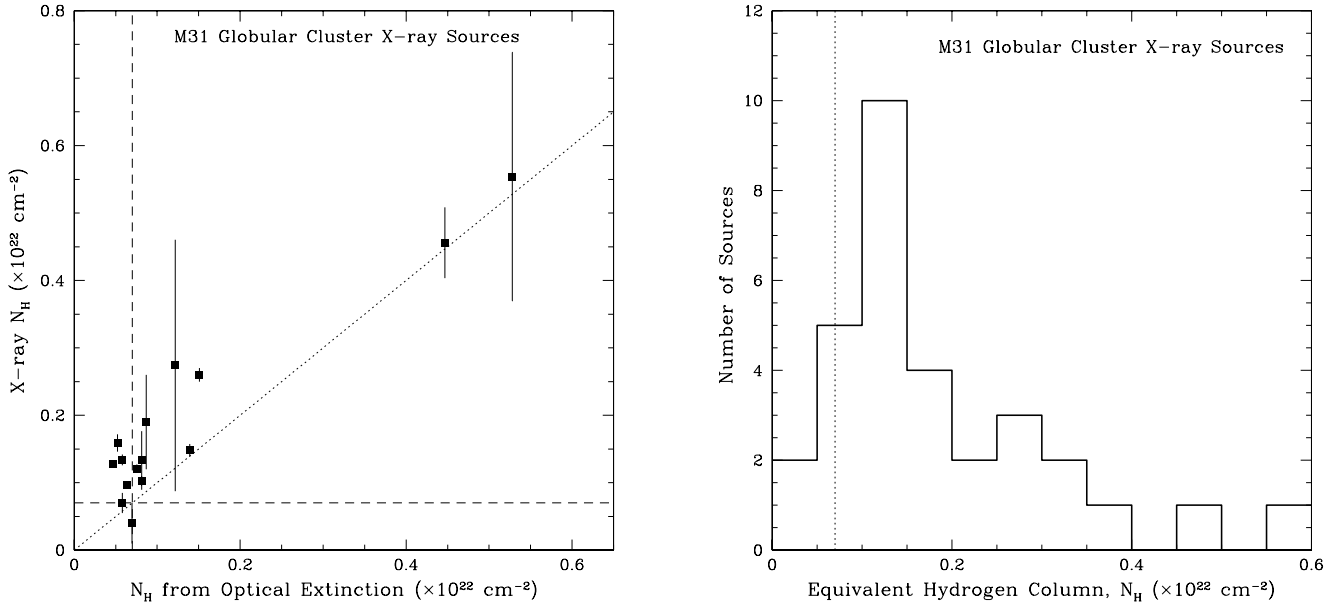

FIG. 7.— *Left panel:* The values of NH derived from X-ray spectral fitting plotted against the values of $N_{\rm H}$ derived from optical extinction data. The dotted line shows points with equal X-ray and optical $N_{\rm H}$. The dashed lines mark expected Galactic foreground absorbing column in the direction of M31. *Right panel:* The distribution of the absorbing columns derived from the spectral analysis of 31 bright GC X-ray sources. Each bin along X-axis has a width of 5×10^{20} cm^{-2}. The Galactic foreground absorbing column in the direction of M31 (7×10^{20} cm^{-2}) is marked with dotted line.

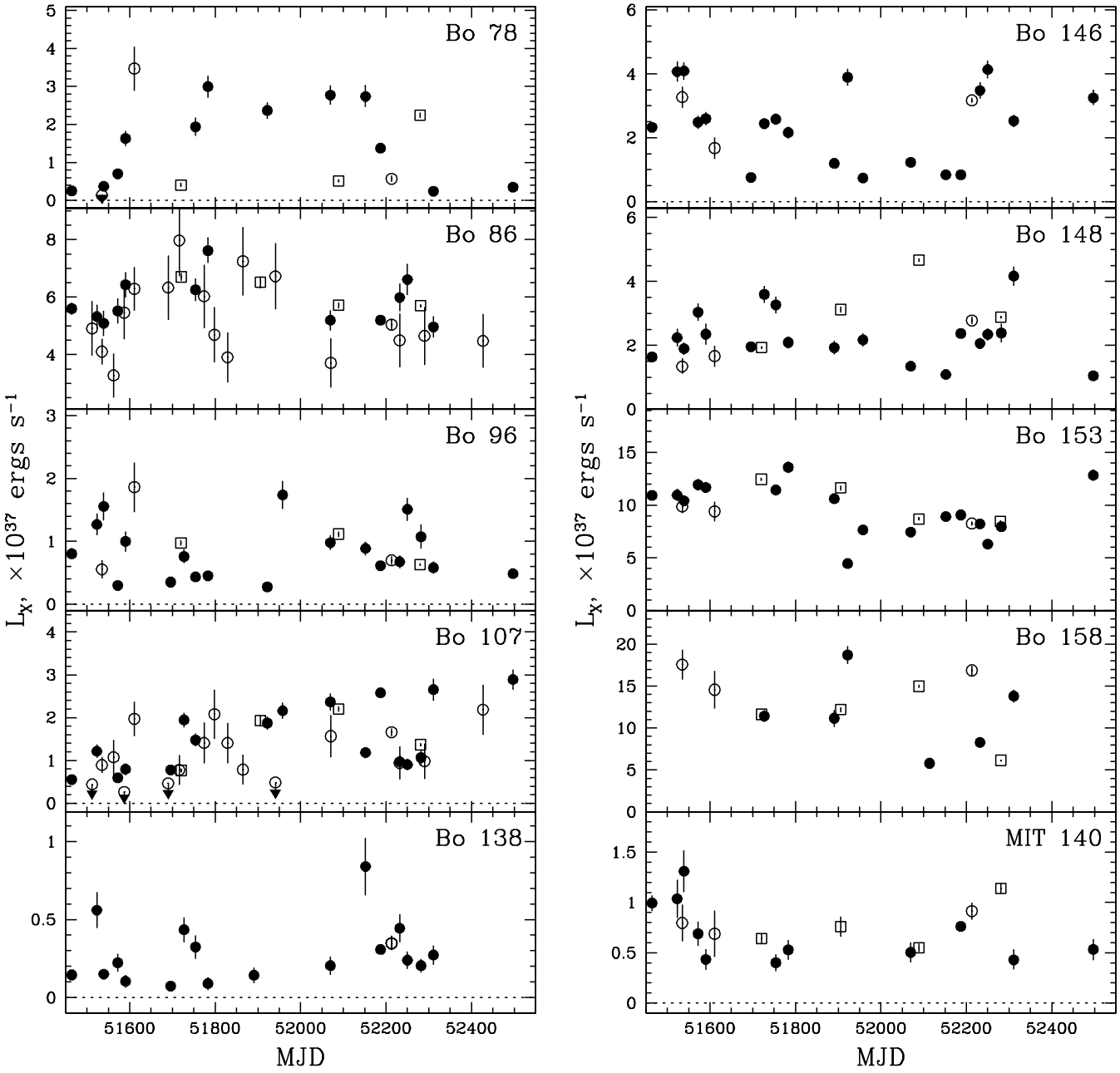

FIG. 8.— X-ray flux histories of 10 GC sources in our sample obtained combining the data of *Chandra*/ACIS (*filled circles*), HRC (*open circles*) and *XMM*/EPIC (*open rectangles*) observations, $0.3-10$ keV energy range. The upper limits correspond to a 2σ level.

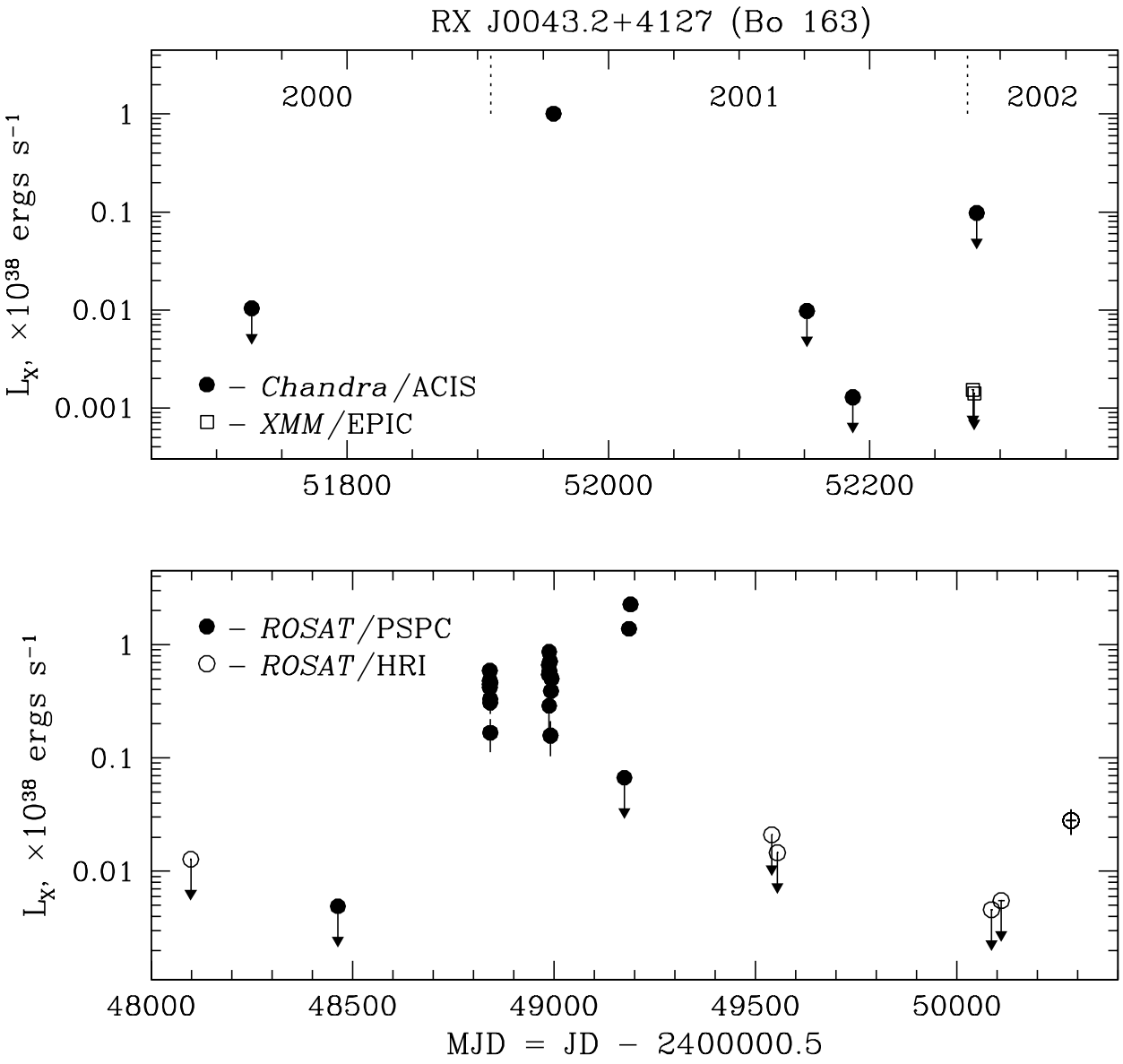

FIG. 9.— X-ray flux histories of the recurrent M31 GC source Bo 163 (#35) based on *XMM-Newton* and *Chandra* (*upper panel*) and *ROSAT* (*lower panel*) archival data. The upper limits correspond to a 2σ level.

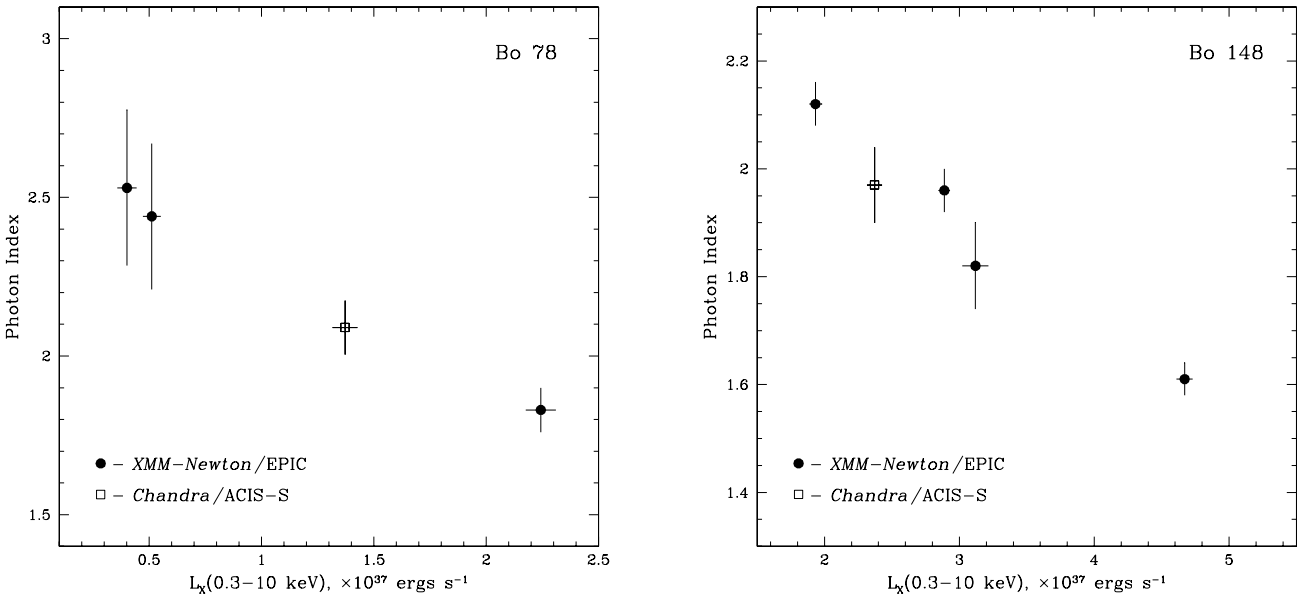

FIG. 10.— Spectral variability of M31 GC sources Bo 78 (#9)(*left panel*) and Bo 148 (#29) (*right panel*). The hardness of the spectrum expressed in terms of the spectral photon index (Y-axis) is plotted against source X-ray luminosity in the $0.3-10$ keV energy band (X-axis).

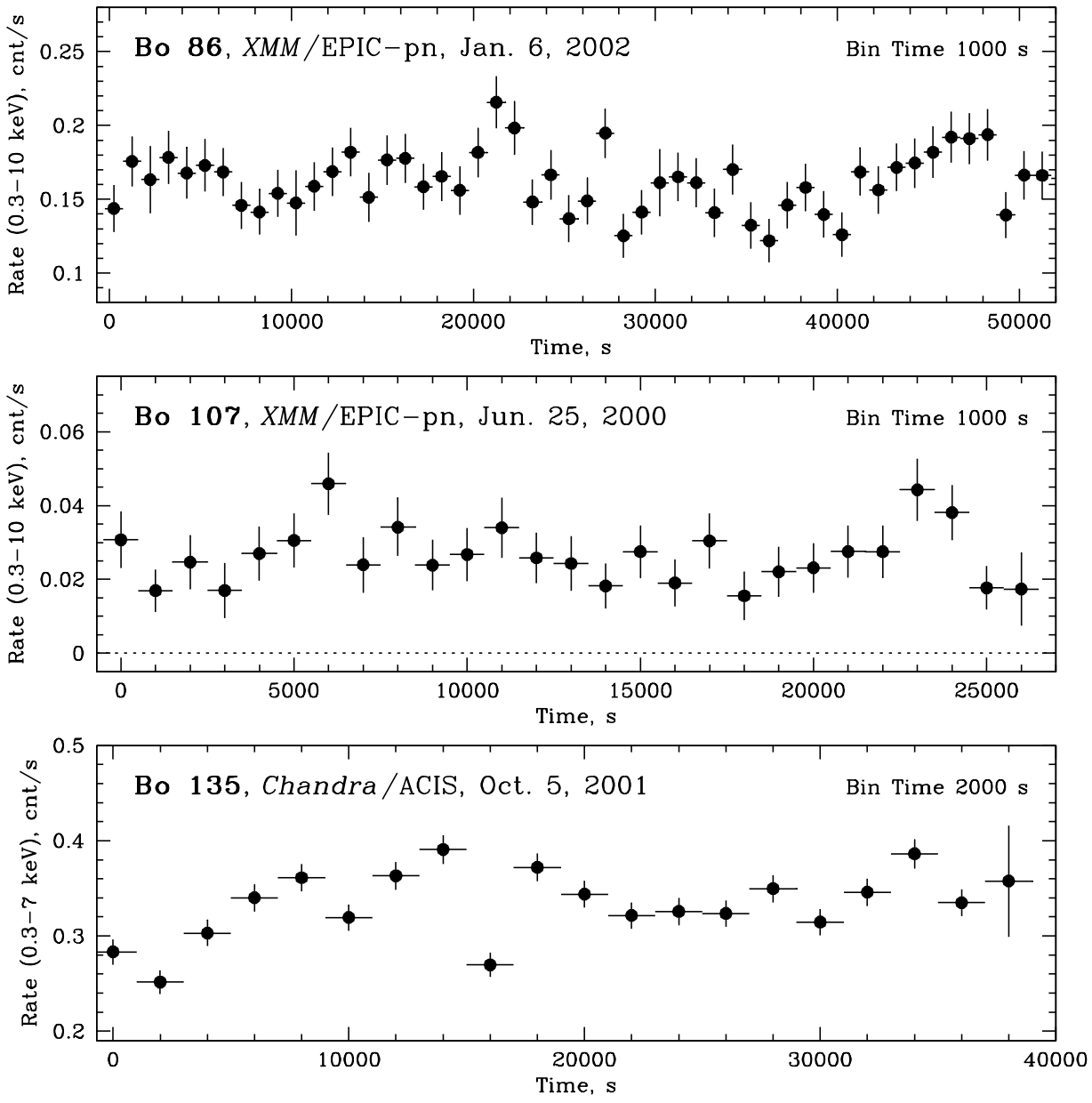

FIG. 11.— *Upper panel:* X-ray light curve of Bo 86 (#11) during the 2002 January 6 *XMM-Newton*/EPIC-pn observation ($0.3-10$ keV energy range and a 1000 s time resolution). *Middle panel:* X-ray light curve of Bo 107 (#16) during the 2000 June 25 *XMM-Newton*/EPIC-pn ($0.3-10$ keV energy range and a 1000 s time resolution). *Lower panel:* X-ray light curve of Bo 135 (#22) during the 2001 October 5 *Chandra*/ACIS observation ($0.3-7$ keV energy range and a 2000 s time resolution).

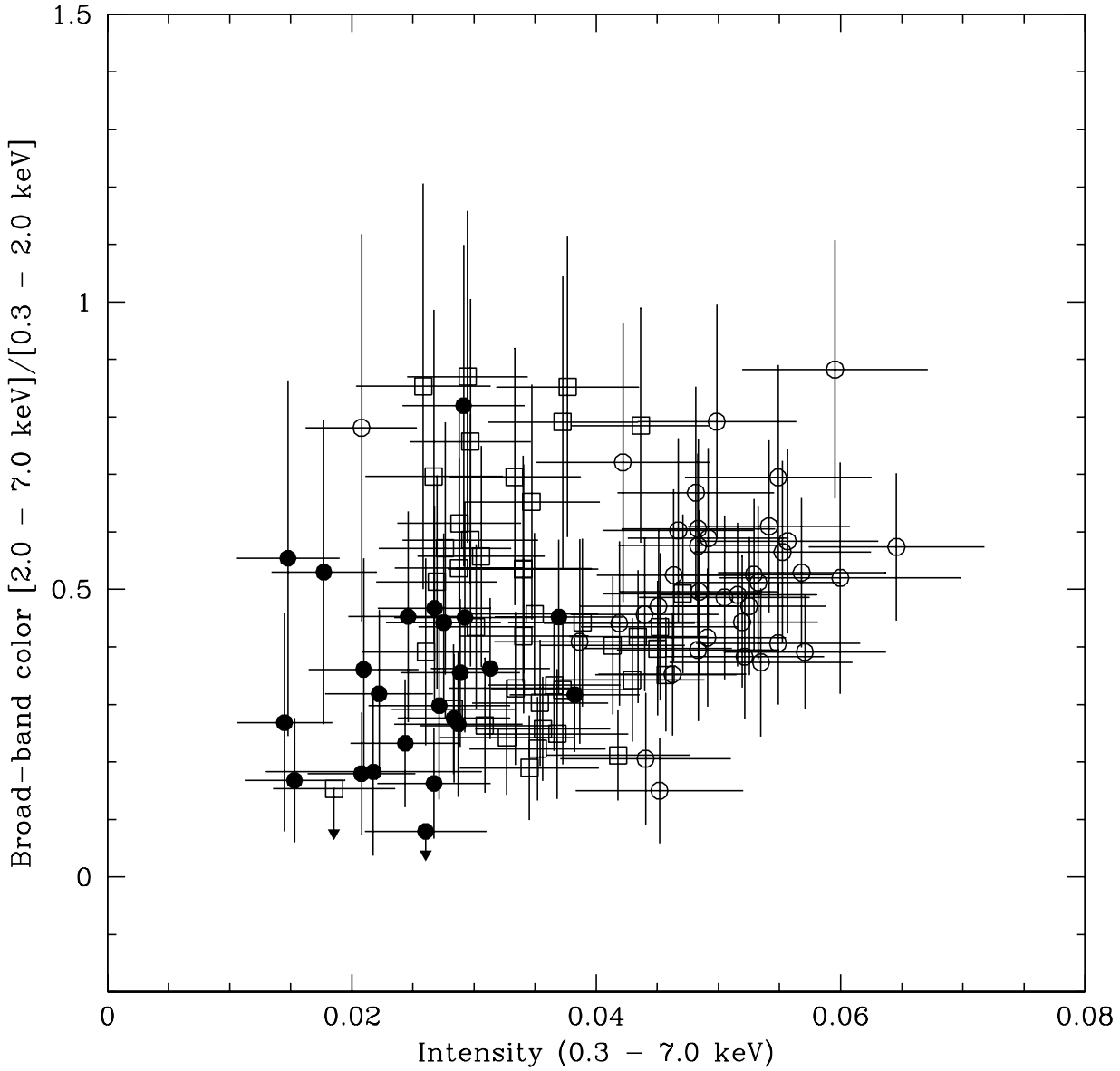

FIG. 12.— Broad-band color (hardness) vs. intensity for three *XMM-Newton* observations of X-ray source in the globular cluster Bo 148 (#29). The broad-band color is defined as ratio of source intensities in the $2.0-7.0$ and $2-7$ keV energy bands. The EPIC-MOS data is binned to 1500 s. The corresponding source luminosity changes between $\sim 10^{37}$ and $\sim 4\times10^{37}$ ergs s^{-1} in the $0.3-10$ keV energy band.

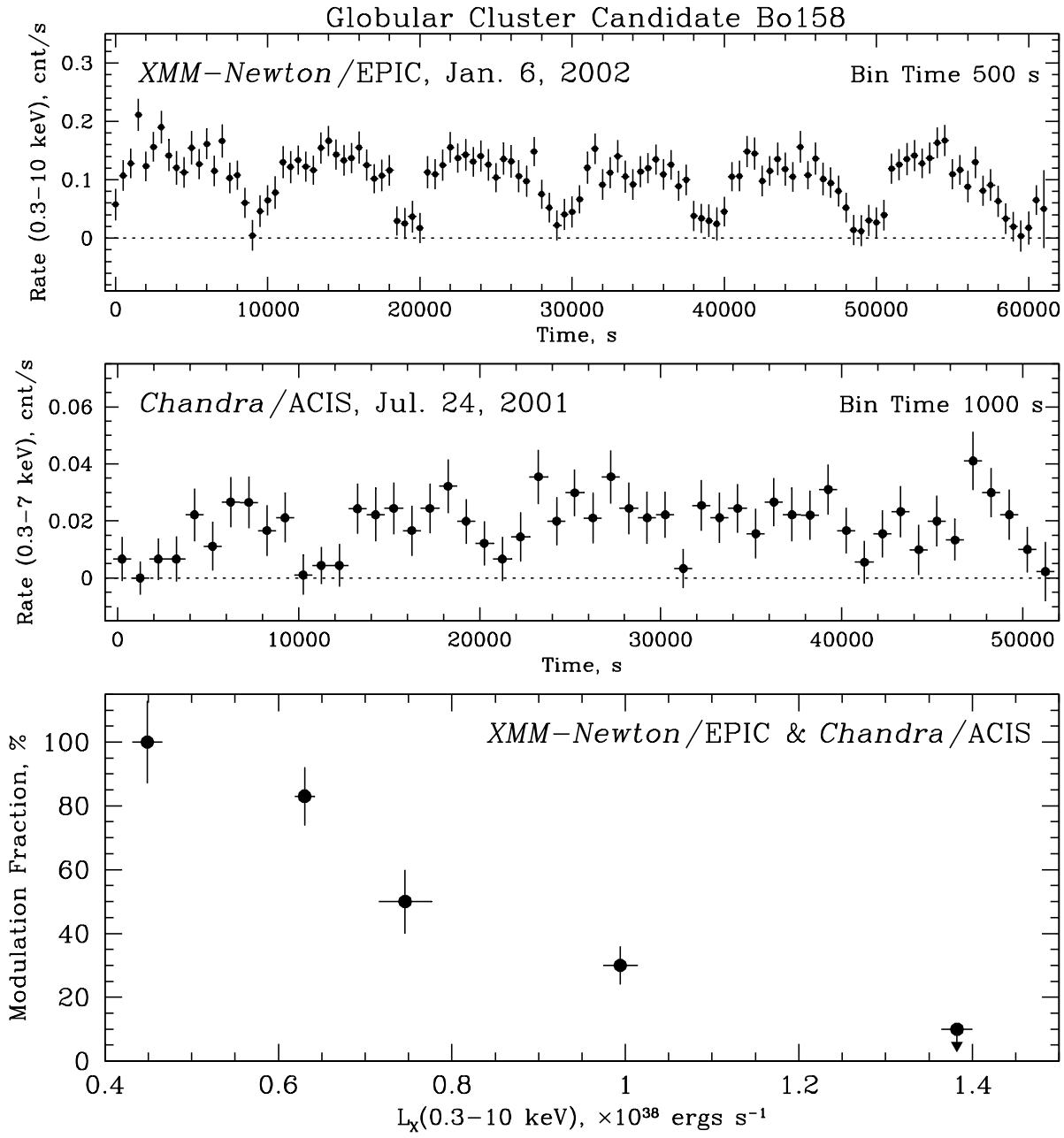

FIG. 13.— *Upper panel:* X-ray light curve of Bo 158 (#32) during the 2002 January 6 *XMM-Newton* observation, obtained from combined EPIC-pn, MOS1, and MOS2 cameras (0.3 − 10 keV energy range and a 500 s time resolution). *Middle panel:* X-ray light curve of Bo 158 during the 2001 July 24 *Chandra*/ACIS observation (0.3 − 7 keV energy range and a 1000 s time resolution). *Lower panel:* The X-ray modulation fraction (%) plotted as a function of X-ray luminosity of Bo 158 (in units of 10^{38} ergs s^{-1})

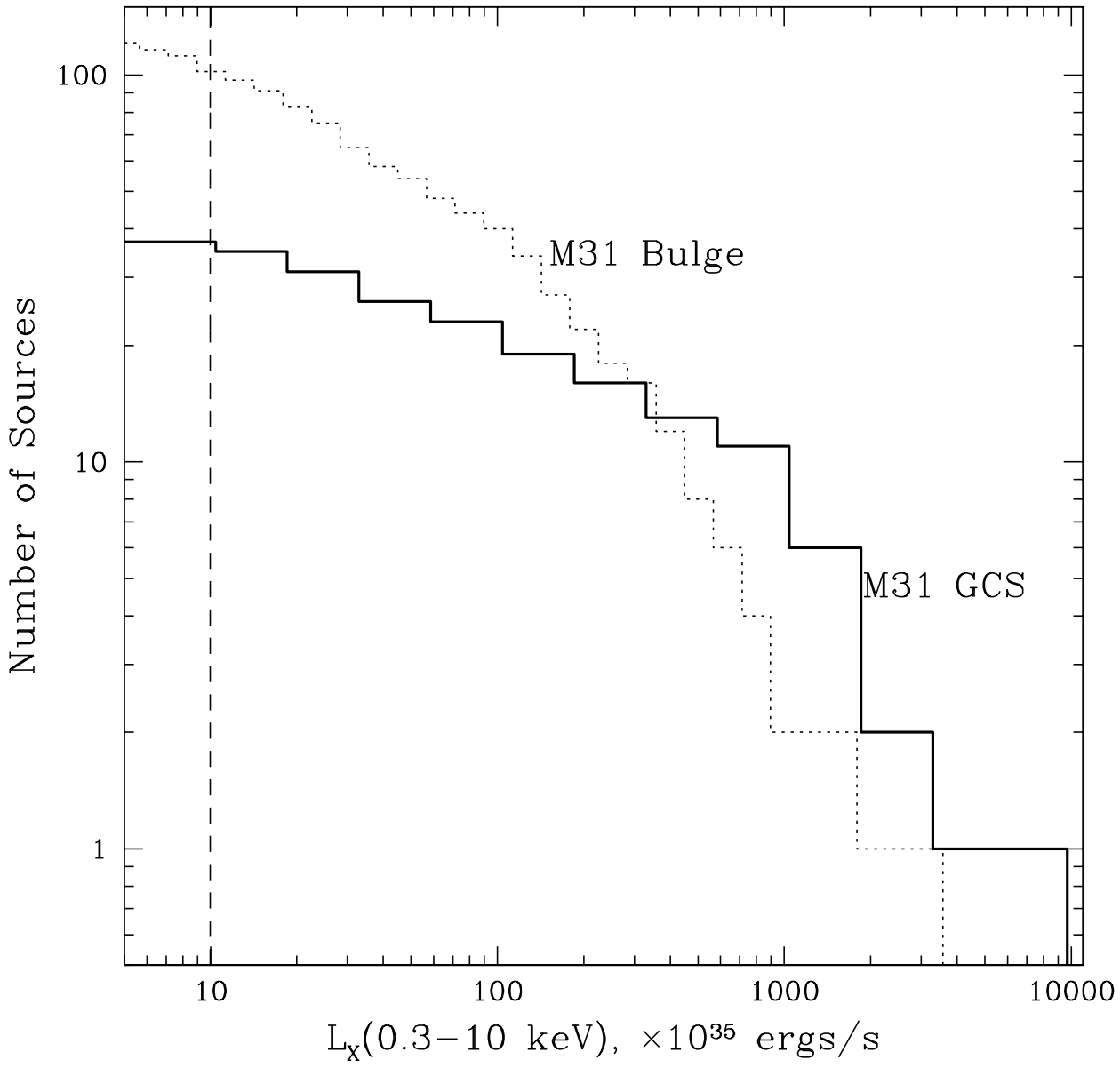

FIG. 14.— Cumulative X-ray luminosity distributions of M31 GC X-ray sources and central bulge of M31.

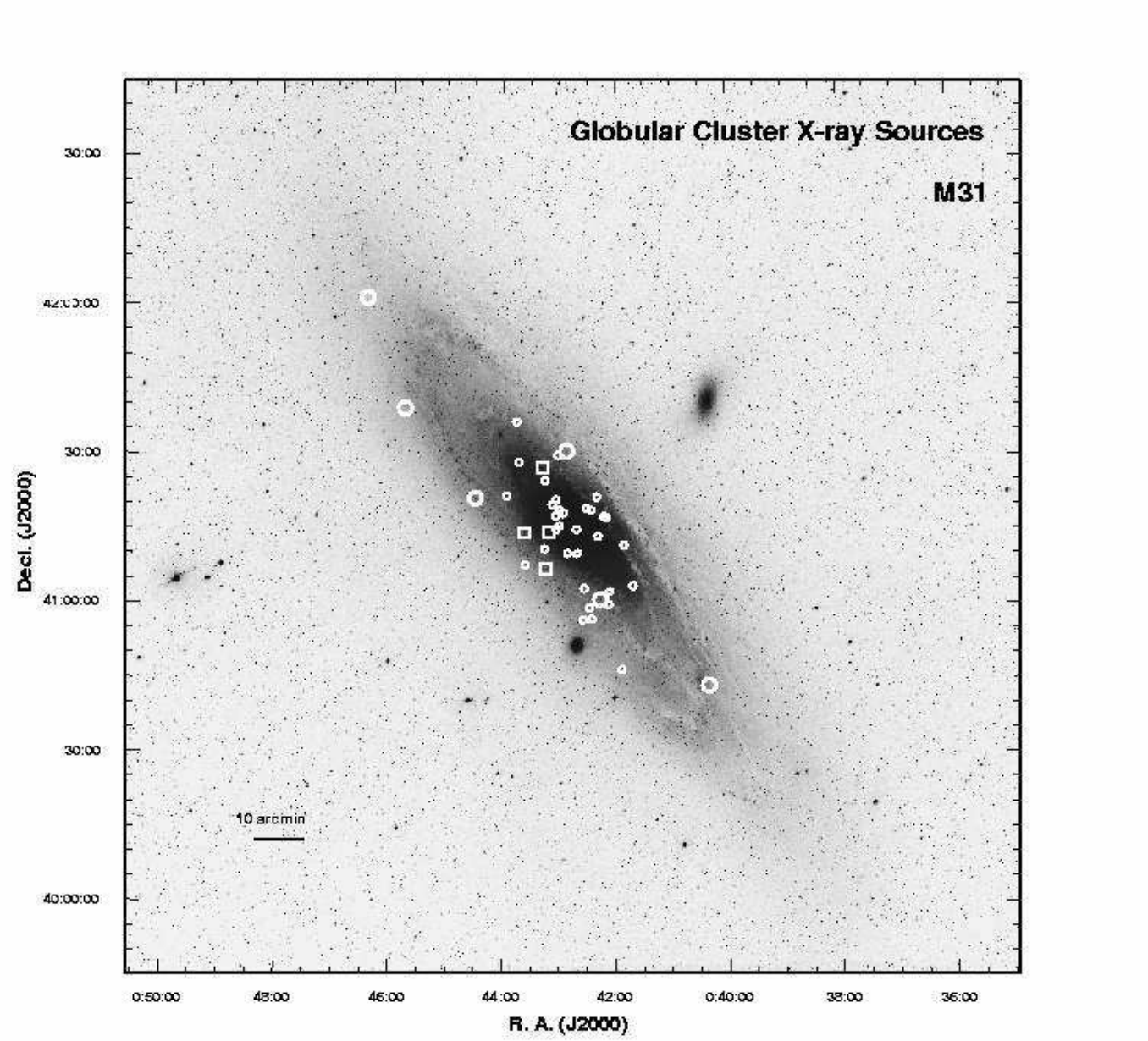

FIG. 15.— Spatial distribution of M31 GC X-ray sources detected with *XMM-Newton* and *Chandra*. The brightest sources with luminosities above 10^{38} ergs s^{-1} are marked with large white circles. X-ray sources with luminosities occasionally exceeding 10^{38} ergs s^{-1} are shown with white boxes. The positions of fainter GC X-ray sources are shown with small white circles.

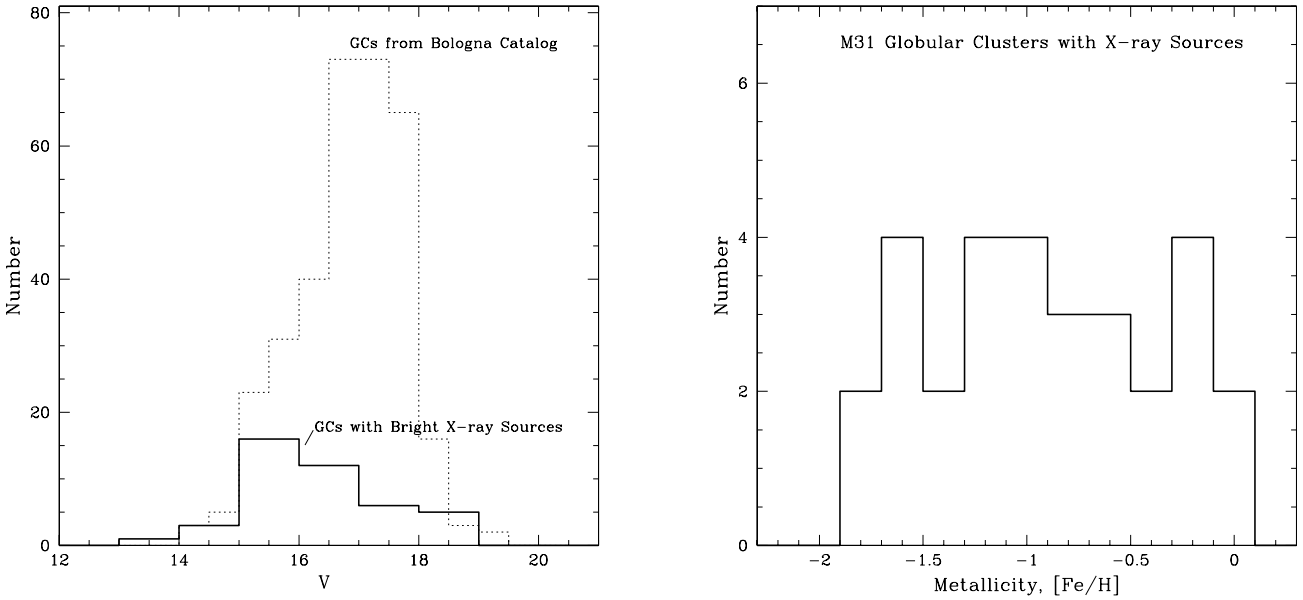

FIG. 16.— *Left panel:* V-magnitude distributions for M31 GC candidates. The results for GC hosting bright X-ray sources are shown with *thick* histogram. The distribution for the GC candidate sample from Battistini et al. 1987 is shown with *dotted* histogram. *Right panel:* metallicity ([Fe/H]) distribution for M31 GC candidates hosting bright X-ray sources.

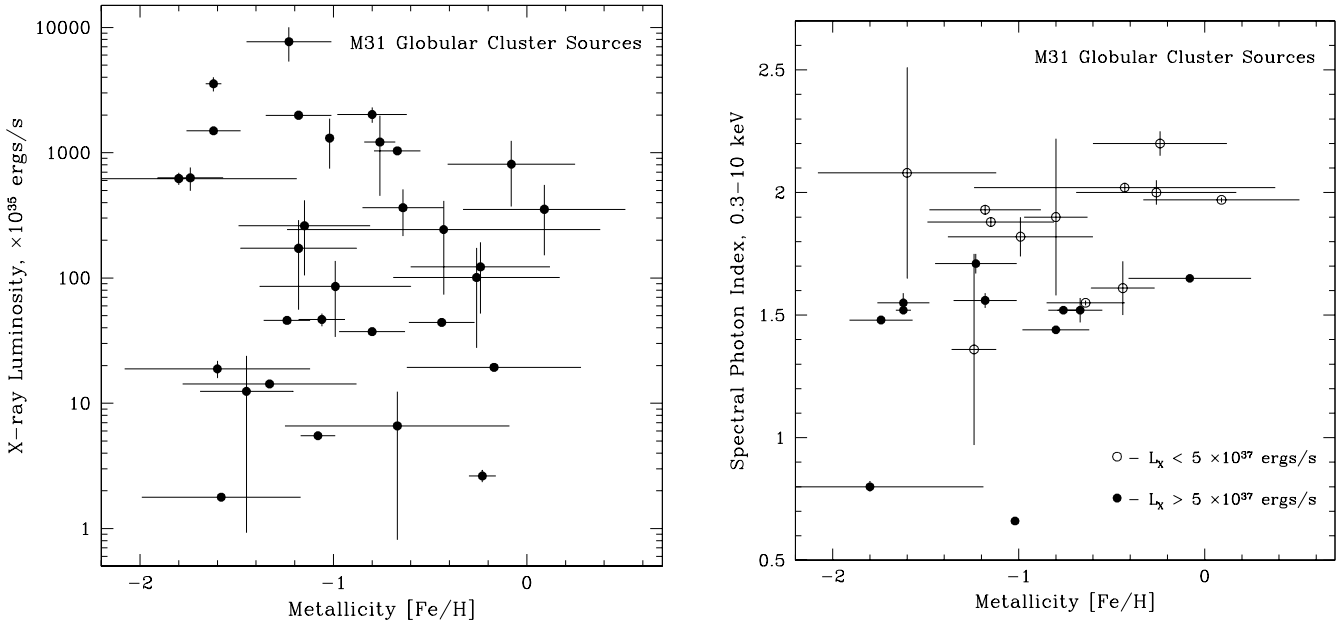

FIG. 17.— *Left panel:* the measured isotropic $0.3 - 10$ keV X-ray luminosity of M31 GC X-ray sources versus the host globular cluster metallicity ([Fe/H]). The error bars in Y-axis reflect statistical uncertainty of the source flux determination and in some cases the range of source X-ray luminosities observed with *XMM* and *Chandra*. *Right panel:* the spectral power law photon index for the GC sources from our sample vs. metallicity of the globular clusters hosting them.